

On the normalised FRB luminosity function

Rui Luo^{1,2}, Kejia Lee[★]^{1,3}, Duncan R. Lorimer^{4,5} and Bing Zhang^{1,2,6}

¹ *Kauli Institute for Astronomy and Astrophysics, Peking University, Beijing 100871, China*

² *Department of Astronomy, School of Physics, Peking University, Beijing 100871, China*

³ *National Astronomical Observatories, Chinese Academy of Sciences, Beijing 100012, China*

⁴ *Department of Physics and Astronomy, West Virginia University, Morgantown, WV 26506, USA*

⁵ *Center for Gravitational Waves and Cosmology, West Virginia University, Chestnut Ridge Research Building, Morgantown, WV 26505, USA*

⁶ *Department of Physics and Astronomy, University of Nevada, Las Vegas, NV 89154, USA*

Accepted XXX. Received YYY; in original form ZZZ

ABSTRACT

Thirty-three fast radio bursts (FRBs) had been detected by March 2018. Although the sample size is still limited, meaningful statistical studies can already be carried out. The normalised luminosity function places important constraints on the intrinsic power output, sheds light on the origin(s) of FRBs, and can guide future observations. In this paper, we measure the normalised luminosity function of FRBs. Using Bayesian statistics, we can naturally account for a variety of factors such as receiver noise temperature, bandwidth, and source selection criteria. We can also include astronomical systematics, such as host galaxy dispersion measure, FRB local dispersion measure, galaxy evolution, geometric projection effects, and Galactic halo contribution. Assuming a Schechter luminosity function, we show that the isotropic luminosities of FRBs have a power-law distribution that covers approximately three orders of magnitude, with a power-law index ranging from -1.8 to -1.2 and a cut off $\sim 2 \times 10^{44} \text{ erg s}^{-1}$. By using different galaxy models and well-established Bayesian marginalisation techniques, we show that our conclusions are robust against unknowns, such as the electron densities in the Milky Way halo and the FRB environment, host galaxy morphology, and telescope beam response.

Key words: stars: luminosity function – cosmology: theory – galaxies: structure – ISM: general

1 INTRODUCTION

Fast Radio Bursts (FRBs) are a new type of radio transients, and remain unexplained. The bursts last for a few milliseconds, and show dispersive signatures with peak flux densities ranging from 0.3 Jy to about 100 Jy. The first one (FRB 010724, Lorimer et al. 2007) was detected serendipitously in the archival data of pulsar survey for Small Magellanic Cloud using the Parkes telescope (Manchester et al. 2006). Shortly after that, a growing number of FRBs were discovered with Parkes at 1.4 GHz, both in the archival data (Keane et al. 2012; Thornton et al. 2013; Burke-Spolaor & Bannister 2014) and from the real-time searches (Ravi et al. 2015; Petroff et al. 2015; Keane et al. 2016; Ravi et al. 2016; Petroff et al. 2017; Bhandari et al. 2018). FRBs were also detected by Arecibo (Spitler et al. 2014), Green Bank Telescope (Masui et al. 2015), UTMOST (Caleb et al. 2017; Farah et al. 2018) and ASKAP

(Bannister et al. 2017). At the time of writing this paper, the total number of the reported detections adds up to 33.

FRBs are natural celestial probes with a broad range of astrophysical applications. For example, it has been proposed that FRBs could be used to test the Einstein’s equivalence principle (Wei et al. 2015; Tingay & Kaplan 2016; Zhang 2016a), to constrain the rest mass of photons (Wu et al. 2016; Bonetti et al. 2016, 2017; Shao & Zhang 2017), to detect the baryon contents in the Universe (McQuinn 2014), to probe the cosmological matter distribution (Masui & Sigurdson 2015), to study the evolution of intergalactic medium (IGM) (Zheng et al. 2014) and constrain the dark-energy equation of states (Zhou et al. 2014; Gao et al. 2014).

The origins of FRBs, however, remain mysterious and subject to an intensive debate. Here, we list several proposals in the literature in chronological order: (1) radio pulses from black hole evaporative explosions (Rees 1977); (2) superconducting cosmic strings (Cai et al. 2012a,b; Yu et al. 2014); (3) flaring magnetars (Popov & Postnov 2010, 2013) or stars (Loeb et al. 2014); (4) mergers of white dwarfs

★ E-mail: kjlee@pku.edu.cn

(Kashiyama et al. 2013); (5) mergers of double neutron stars (Totani 2013; Wang et al. 2016); (6) collapses of neutron stars into black holes (Falcke & Rezzolla 2014; Zhang 2014); (7) synchrotron masers (Lyubarsky 2014; Ghisellini 2017; Lu & Kumar 2018); (8) binary model of white dwarf and black hole (Gu et al. 2016); (9) super-giant pulses from pulsars (Cordes & Wasserman 2016; Connor et al. 2016); (10) radio emission from soft gamma-ray repeaters (Pen & Connor 2015; Katz 2016); (11) axion stars (Iwazaki 2015); (12) quark nova (Shand et al. 2016); (13) mergers of charged black holes (Zhang 2016b; Liu et al. 2016); (14) collisions between pulsar and asteroids (Geng & Huang 2015; Dai et al. 2016); (15) relativistic jet – cloud interactions (Romero et al. 2016; Vieyro et al. 2017); (16) births of millisecond magnetars (Metzger et al. 2017); (17) ‘cosmic comb’, i.e. magnetosphere – environment interactions (Zhang 2017, 2018b); (18) accretion of black holes (Katz 2017); (19) star-quakes of compact stars (Wang et al. 2018).

To understand the mechanisms of FRBs, the host galaxy information is crucial. At this stage, only the repeating FRB, FRB 121102, had the reliable identification of host galaxy (Spitler et al. 2016; Scholz et al. 2016). Chatterjee et al. (2017) measured its precise position using *Karl G. Jansky Very Large Array*. The optical counterpart was identified as a dwarf galaxy at the redshift of $z = 0.193$ (Tendulkar et al. 2017). However, we should be cautious in drawing general remarks on the FRB environment, due to unknown links between repeating and non-repeating FRBs. Statistical analyses are needed to quantify the properties of FRBs as an integrated population.

The normalised luminosity function, i.e. the probability density function (PDF) of FRB luminosities, is one particularly important statistics for the FRB intrinsic power output. The computation of the luminosity functions requires not only FRB flux and distances, but also a detailed account of any biases in the sample. For example, without the counterpart identifications, the FRB distances are usually estimated via the dispersion measure (DM). The estimated FRB distance and luminosity are affected by the uncertainties in the DM modelling. It is absolutely necessary to account for these effects in inferring the luminosity function.

There are several algorithms to measure the luminosity function (see Willmer (1997) for a review). The non-parametric methods (e.g. Lynden-Bell 1971) usually require certain uniformity of data coverage to be applicable. The likelihood-based methods (Marshall et al. 1983) or Bayesian methods (Kelly et al. 2008; Chennamangalam et al. 2013) are preferable for the FRB problems, because these algorithms are more flexible in modelling the systematics and less constrained by the conditions of a given sample.

In this paper, we aim to measure the normalised FRB luminosity function. To include systematics and unknowns in the statistical inference, we develop a Bayesian framework suitable for the current problem. For most of the known FRBs, there are four main observables relevant to the luminosity function determination: flux density, bandwidth, duration, and dispersion measure. Compared to the other astronomical sources whose luminosity functions are measured, the FRB distance is not directly available. As a result, we have to rely on the dispersion measure to indirectly infer the FRB distance. Our method to measure the FRB luminosity function includes three major steps: (1) mitigate

the Galactic foreground contribution of the dispersion measure; (2) model the FRB host galaxy and the cosmological dispersion measure contribution; (3) include dispersion measure models in the Bayesian luminosity function inference, and marginalise the unknowns. The first step is straightforward, as good knowledge on the Galactic electron distribution is available. The second step is to model the effects of some unknown properties on determining the luminosity function. The third step is to use a Bayesian method developed in this paper to ‘enumerate’ all possibilities and include the unknowns in the statistical inference. We can then determine the contribution of the unknowns to statistical errors, e.g. we can make sure that the confidence bounds of inferred parameters contain the uncertainties in the modelling.

The paper is organised as follows. In Section 2, we explain how we remove the dispersion measure contribution from the Galactic foreground. In Section 3, we describe our Bayesian inference method. The likelihood function is built in Section 3.1, with detailed modelling of its components in the rest of the subsections of Section 3. The computational method for posterior evaluation is shown in Section 3.5. Our results are given in Section 4, with discussion made in Section 5. For the readers’ convenience, we summarise the symbols used throughout this paper in Table A1.

2 PRE-PROCESSING THE FRB DATA

For most FRBs, the measured parameters are peak flux density (S_{peak}), burst duration (w), and dispersion measure

$$\text{DM} = \int n_e dl, \quad (1)$$

i.e., the electron density n_e integrated along the line of sight, which serves as the distance indicator for the FRBs.

When radio waves propagate through interstellar medium (ISM), the group velocity becomes frequency-dependent (Landau & Lifshitz 1960). For the rest-frame observer, the time delay between the pulses at two different frequencies is

$$\Delta t = 4.15 \text{ ms} \left(\frac{\text{DM}}{1 \text{ cm}^{-3} \text{ pc}} \right) \left[\left(\frac{\nu_1}{1 \text{ GHz}} \right)^{-2} - \left(\frac{\nu_2}{1 \text{ GHz}} \right)^{-2} \right], \quad (2)$$

under the assumption that the radio wave frequency is higher than the ISM plasma frequency. The DMs are then usually measured by fitting the observed time delays using Equation (2).

All the data used in this paper comes from the FRB catalogue (FRBCAT)¹ compiled by Petroff et al. (2016) amended with the original discovery papers. In Table B1 of Appendix B, We list the values of the observed and inferred parameters of FRBs used in the current paper for reader’s reference.

The DM of an FRB has contributions from five components, i.e.

$$\text{DM} = \text{DM}_{\text{MW}} + \text{DM}_{\text{halo}} + \text{DM}_{\text{IGM}}(z) + \frac{\text{DM}_{\text{host}} + \text{DM}_{\text{src}}}{1 + z}. \quad (3)$$

In the above expression DM_{MW} is the component due to the Milky Way free electrons, DM_{halo} is the possible component

¹ <http://frbcatalog.org/>

contributed by the electron halo of the Milky Way, DM_{IGM} is the intergalactic medium (IGM) contribution, DM_{host} is the FRB host galaxy contribution, and DM_{src} is the component from the local environment surrounding the FRB source in small scales, e.g. HII regions, ionised gas halos, magnetospheres. The cosmological redshift factor, $1+z$, converts the DM seen by the rest-frame observer to that of the Earth observer as shown by Deng & Zhang (2014).

There are currently two models that are widely used for the Galactic distribution of free electrons: NE2001 (Cordes & Lazio 2002), and YMW16 (Yao et al. 2017). The NE2001 model contains several components for the electron density distribution, the thin and thick asymmetric disks, the spiral arms, a local arm, a local hot bubble surrounding the Sun, and relatively large super-bubbles in the first and third Galactic quadrants. It also includes over dense components representing the small scale structures. By contrast, the more recent YMW16 model contains a four-armed spiral pattern together with the local structures similar to that of NE2001. YMW16 does not include the clumps or voids to correct for DMs of individual pulsars, but more pulsars with independent distance measurements were used in fitting the model parameters. Compared with that of NE2001, the average electron density of YMW16 is lower (Yao et al. 2017).

In our data preprocessing, we remove the Milky Way contribution from the observed DM of each FRB to get the extragalactic contribution based on two representative models described above (i.e. the NE2001 and YMW16). The observed DM as well as the extragalactic DM (DM_{E}), i.e. $DM_{\text{E}} = DM - DM_{\text{MW}}$, are listed in Table B1. As one can see, most of the extragalactic DM values are compatible between the two Galactic electron models; Only for certain FRBs, e.g. FRB 010621, there is a factor-of-two difference.

The Milky Way dark halo may contribute to the DM. The standard picture (Sembach et al. 2003; Bregman & Lloyd-Davies 2007; Gaensler et al. 2008), however, indicates a very low electron density ($n_{\text{e}} < 10^{-3} - 10^{-4} \text{ cm}^{-3}$) in the extended Milky Way halo with typical predictions of $DM_{\text{halo}} \simeq 30 \text{ cm}^{-3} \text{ pc}$ (Dolag et al. 2015). We compare the results with and without correcting the halo contribution in Section 4, i.e. the results using $DM_{\text{E}} = DM - DM_{\text{MW}} - DM_{\text{halo}}$ and $DM_{\text{E}} = DM - DM_{\text{MW}}$. The negligible difference in the results legitimate performing the halo correction in the pre-processing stage *a posteriori* and save us from the complex probabilistic modelling. However we are not that lucky for other systematics, which requires proper modelling as shown in the next section.

3 BAYESIAN FRAMEWORK TO MEASURE THE FRB LUMINOSITY FUNCTION

We develop a Bayesian data analysis scheme to measure the luminosity function of known FRBs from three observables, the peak flux density, the burst duration and the extragalactic DM. These observables are insufficient to directly compute the FRB luminosity, because the FRB distance and DM do not fall into the one-to-one relation. In order to measure the luminosity function, we seek help from the Bayesian method, which can include the systematics of the unknowns. Bayesian inference (see, e.g., Jaynes 2003, for details) helps

to convert the ‘probability of data’ to the ‘probability of parameters’ via Bayes’ theorem,

$$P(\Theta|\mathbf{X}) = \frac{P(\Theta)P(\mathbf{X}|\Theta)}{P(\mathbf{X})}, \quad (4)$$

where \mathbf{X} represents the *data*, and Θ is a vector set of model *parameters* to be inferred. The *likelihood* function, $\Lambda \equiv P(\mathbf{X}|\Theta)$, is the PDF of the data given the model parameters. $P(\Theta|\mathbf{X})$ is the *posterior* PDF, i.e. the PDF for the parameters given the data set. The Bayesian *evidence* $P(\mathbf{X})$ is a normalization coefficient that

$$P(\mathbf{X}) = \int \mathbf{P}(\Theta)\mathbf{P}(\mathbf{X}|\Theta)d\Theta. \quad (5)$$

The *prior* PDF $P(\Theta)$ describes our information *a priori* about the model parameters. In the current paper, the data \mathbf{X} are the measured FRB parameters (i.e. DM_{E} , S_{peak} , and w), and the parameters Θ are for the luminosity function. In the common practice of Bayesian data analysis, one needs to construct the likelihood function and compute the posterior to infer the parameters.

3.1 Likelihood function

We construct the likelihood function under six assumptions.

i) The FRB luminosity distribution follows the Schechter function (Schechter 1976), which was widely used for galaxies, quasars and gamma-ray bursts. It takes the form of

$$\phi(\log L)d \log L = \phi^* \left(\frac{L}{L^*} \right)^{\alpha+1} e^{-\frac{L}{L^*}} d \log L, \quad (6)$$

where ϕ^* is the normalisation factor, α is the power-law index of the distribution and L^* is the cut-off luminosity. There are two considerations to use the Schechter function. Firstly, the function includes a common power-law function with the inclusion of an exponential cut-off. In the régime $L < L^*$, the function is consistent with a power law. The cutoff ensures that there exists a maximal luminosity of FRBs. Second, such a function has been used in describing the luminosity functions of other astrophysical objects.

ii) The cosmological evolution of FRB luminosity function can be neglected, in other words, the parameters in the Schechter function are independent of redshift.

iii) The spatial distribution of FRBs is homogeneous in the comoving volume, i.e. the PDF for the comoving radius r proportional to the differential comoving volume, i.e. $f_i(r) \propto dV/dr \propto r^2$. As a caveat, it is well known (Binggeli et al. 1988) that the source may not be perfectly homogeneous in the comoving volume. Particularly, one needs to factor in the effects of luminosity function and redshift distribution (see Equation (15) in Binggeli et al. (1988)). However, we had only the limited number of FRBs, the homogeneous assumption is a valid ‘first-order’ approximation. Tests for homogeneity are only possible when a sufficient number of FRBs are detected.

iv) The luminosity distribution of FRBs is independent of FRB positions in their host galaxies.

v) The source DM contribution (DM_{src}) is independent of the host galaxy dispersion measure and the FRB luminosity, i.e. DM_{src} is independent of DM_{host} and L . Here, the DM_{src} is dedicated to the local environment of FRBs,

of which the sizes are much smaller than the host galaxy. The host-galaxy-dependant DM in our modelling is through DM_{host} as discussed in Section 3.4.

vi) The FRB true position distributes uniformly (per solid angle) inside the telescope main beam. The off-centre position introduces a lower beam response with $\epsilon \leq 1$ (See Section 3.2)

With the above six assumptions, FRB luminosity (L), comoving radius (r), host galaxy DM, FRB local DM (DM_{src}), and beam response (ϵ) become independent random variables. Thus the joint PDF becomes multiplicative, i.e

$$f(\log L, r, \text{DM}_{\text{host}}, \text{DM}_{\text{src}}, \log \epsilon) = \phi(\log L) f_r(r) f_{\mathcal{D}}(\text{DM}_{\text{host}}|z) \times f_s(\text{DM}_{\text{src}}) f_{\epsilon}(\log \epsilon) \quad (7)$$

where f_s is the PDF of DM_{src} , and f_{ϵ} is the PDF of beam response of radio telescope. The free electron density in the host galaxies highly depends on the star formation activity, which is roughly reduced by a factor of 10 from redshift $z = 1$ to $z = 0$ (Hopkins & Beacom 2006; Madau & Dickinson 2014). The PDF $f_{\mathcal{D}}(\text{DM}_{\text{host}}|z)$ for the rest-frame DM_{host} becomes redshift dependent.

To compute the likelihood, we need to obtain the PDF of the observables. This can be done by the nonsingular random variables transformation (Fisz 1963). We map the PDF of quintet $\{\log L, r, \text{DM}_{\text{host}}, \text{DM}_{\text{src}}, \log \epsilon\}$ to that of $\{\log S, \text{DM}_{\text{E}}, z, \text{DM}_{\text{src}}, \log \epsilon\}$ using the Jacobian transformation. As a nonsingular transformation, one has

$$f(\log S, \text{DM}_{\text{E}}, z, \text{DM}_{\text{src}}, \log \epsilon) = \left| \frac{\partial(\log L, r, \text{DM}_{\text{host}}, \text{DM}_{\text{src}}, \log \epsilon)}{\partial(\log S, \text{DM}_{\text{E}}, z, \text{DM}_{\text{src}}, \log \epsilon)} \right| \times f(\log L, r, \text{DM}_{\text{host}}, \text{DM}_{\text{src}}, \log \epsilon). \quad (8)$$

The Jacobian determinant is calculated using the luminosity-flux and $\text{DM}_{\text{E}}(\text{DM}_{\text{host}}, \text{DM}_{\text{src}})$ relations as follows.

The apparent flux density is determined by source luminosity and beam response, i.e.

$$\log S = \log L - 2 \log r_{\text{L}} - \log \Delta \nu_0 + \log \epsilon - \log 4\pi, \quad (9)$$

$$r_{\text{L}} = (1+z)r, \quad (10)$$

$$r = \frac{c}{H_0} \int_0^z \frac{1}{E(z)} dz. \quad (11)$$

Here we assume the intrinsic spectrum of FRB is flat, and the spectral width $\Delta \nu_0$ is fixed to the reference values of 1 GHz. The Hubble constant is taken as $H_0 = 67.8 \text{ km s}^{-1} \text{ Mpc}^{-1}$ (Planck Collaboration et al. 2016). The luminosity distance, r_{L} , is computed from the comoving distance, r . The function

$$E(z) = \sqrt{\Omega_{\text{m}}(1+z)^3 + \Omega_{\Lambda}} \quad (12)$$

is the logarithmic time derivative of the cosmic scale factor in a flat Λ CDM universe ($\Omega_k \simeq 0$), in which we adopt dimensionless matter density $\Omega_{\text{m}} = 0.308$ and cosmological constant $\Omega_{\Lambda} = 0.692$ (Planck Collaboration et al. 2016).

The intrinsic DM from the host galaxy is calculated by subtracting the IGM and source contributions from the extragalactic DM, i.e.

$$\text{DM}_{\text{host}} = (\text{DM}_{\text{E}} - \text{DM}_{\text{IGM}})(1+z) - \text{DM}_{\text{src}}, \quad (13)$$

where the factor $(1+z)$ comes from converting the DM seen by the Earth observer to the DM seen by the FRB rest-frame observer (Ioka 2003; Inoue 2004). The electron density of IGM depends on the ionization history of the Universe (Deng & Zhang 2014, see also Appendix E)

$$\text{DM}_{\text{IGM}} \simeq 1.1 \times 10^3 \int_0^z \frac{f_{\text{IGM}} g(z)(1+z) dz}{E(z)} \text{ cm}^{-3} \text{ pc}, \quad (14)$$

where the f_{IGM} is the cosmological baryon mass fraction in the IGM, here we adopt $f_{\text{IGM}} \simeq 0.83$ from the summation of global budget of baryons in all states (Fukugita et al. 1998). The function $g(z)$, on the right hand of Equation (14), is the ionised electron number fraction per baryon. One has

$$g(z) \simeq \frac{3}{4} \chi_{e,\text{H}}(z) + \frac{1}{8} \chi_{e,\text{He}}(z), \quad (15)$$

where $\chi_{e,\text{H}}$ and $\chi_{e,\text{He}}$ are the cosmic ionisation fraction of hydrogen and helium, respectively. FRBs are located relatively nearby, so that one can safely adopt $\chi_{e,\text{H}} \simeq 1$ and $\chi_{e,\text{He}} \simeq 1$ (Fan et al. 2006; McQuinn et al. 2009).

Using Equation (9), (10) and (13), we calculate the Jacobian determinant in Equation (8). After marginalisation of DM_{src} and ϵ , the PDF $f(\log S, \text{DM}_{\text{E}}, z)$ becomes (see Appendix C for details).

$$f(\log S, \text{DM}_{\text{E}}, z) = I(\log L) f_z(z) I(\text{DM}_{\text{E}}, z)(1+z), \quad (16)$$

where the marginalisations for the unknown source DM (DM_{src}) and beam response (ϵ) are

$$I(\text{DM}_{\text{E}}, z) \equiv \int_0^{\max(\text{DM}_{\text{src}})} f_{\mathcal{D}}(\text{DM}_{\text{host}}|z) f_s(\text{DM}_{\text{src}}) d\text{DM}_{\text{src}}, \quad (17)$$

and

$$I(\log L) \equiv \int \phi(\log L) f_{\epsilon}(\log \epsilon) d \log \epsilon \quad (18)$$

Since only one FRB has a measured redshift so far, we need to marginalise the redshift in the likelihood to include such an ignorance. The reduced likelihood function, as what will be used in the Bayesian inference, is

$$f(\log S, \text{DM}_{\text{E}}) = \frac{1}{N_f} \int_0^{\infty} I(\log L) f_z(z) I(\text{DM}_{\text{E}}, z)(1+z) dz, \quad (19)$$

where $f_z(z)$ is the FRB spatial distribution function in the redshift space with

$$f_z(z) = \frac{r(z)^2}{E(z)}, \quad (20)$$

and N_f is the normalisation factor as

$$N_f = \int_{\log S_{\text{min}}}^{\infty} d \log S \int \int f(\log S, \text{DM}_{\text{E}}, z) d\text{DM}_{\text{E}} dz. \quad (21)$$

The lower limit of the flux density integration, S_{min} , is the minimum detectable flux density of the telescope at the time when the given FRB was detected, i.e. the survey depth. The radiometer equation (Lorimer & Kramer 2012) gives

$$S_{\text{min}} = \frac{S/N_0 T_{\text{sys}}}{G \sqrt{N_p} \text{BW} w} = \frac{S/N_0 \text{SEFD}}{\sqrt{N_p} \text{BW} w}, \quad (22)$$

where w is the FRB pulse width, S/N_0 is the signal-to-noise ratio threshold for detection in the surveys, T_{sys} is the system temperature, G is the telescope gain, N_p is the number

Table 1. The instrumental parameters of FRB surveys

Survey	G K/Jy	$T_{\text{sys}}^{\text{a}}$ K	SEFD Jy	BW MHz	S/N ₀	N_{p}	Ref. ^b
Parkes I	0.69	28	41	288	7	2	[1]
Parkes II	0.69	28	41	338	10	2	[2]
Arecibo	0.7 ^c	30	43	322	7	2	[3]
GBT	2.0	25	13	200	8	2	[4]
UTMOST	3.0	400	130	16	10	1	[5]
ASKAP	n/a	n/a	1800	336	10	2	[6]

(a) For different FRB detections, the telescope system temperatures depend on the detected beams. Hence, in the calculation for sensitivity of each FRB, we adopted the corresponding value from the newest FRBCAT.

(b) The references are: [1] Lorimer et al. (2007); [2] Thornton et al. (2013); [3] Spitler et al. (2014); [4] Masui et al. (2015); [5] Caleb et al. (2017); [6] Bannister et al. (2017).

(c) The Arecibo FRB was detected probably in the sidelobe of multi-beam receiver, the gain of sidelobe is taken as 0.7 K/Jy (Spitler et al. 2014).

of polarisations summed, and BW is the bandwidth. The system temperature and gain can be combined using the system equivalent flux density (SEFD $\equiv T_{\text{sys}}/G$) as shown on the right-hand side of Equation (22). The parameters for the depths of surveys are given in Table 1, the numeric values of the corresponding parameters are from the reference listed in Table B1.

We need to model the beam response $f_{\epsilon}(\log \epsilon)$, local DM and host galaxy DM distribution function $f_{\text{s}}(\text{DM}_{\text{src}})$ and $f_{\mathcal{D}}(\text{DM}_{\text{host}}|z)$ before computing the likelihood. The modelling will be explained in the next sections.

3.2 The beam response likelihood

We can approximate the main-beam response using a Gaussian function (Born & Wolf 1999), where the ratio between the observed flux and the intrinsic flux of an FRB,

$$\epsilon \equiv \frac{S_{\text{obs}}}{S_{\text{src}}} = e^{-4 \ln 2 \left(\frac{\theta}{\theta_{\text{b}}} \right)^2}. \quad (23)$$

In this expression, S_{src} and S_{obs} are the true and observed flux of FRB. θ is the angular distance between the true position of FRB and the beam centre. θ_{b} is the full-width-half-maximum (FWHM) beam size, i.e. $\epsilon = 0.5$ for $\theta = \theta_{\text{b}}/2$.

If we assume a uniform PDF per solid angle for the source position inside the main beam, i.e. accepting Assumption vi) made in Section 3.1, the PDF of $\cos \theta$ will also be uniform. For most of the radio telescopes, if not all, $\theta_{\text{b}} \ll 1$ rad, so does θ , including the telescopes that have beams with large semi-major axis and small semi-minor axis, e.g. UTMOST. Thus θ^2 also follows a uniform PDF. As $\log \epsilon \propto -\theta^2$, the PDF of $\log \epsilon$ is uniform as well. We get $f_{\epsilon}(\log \epsilon) = \text{constant}$.

3.3 The distribution function for the local DM of the FRB source

The nature of FRB origins is still under debate and the PDF of FRB local DM is highly uncertain. Investigations

(Yu 2014; Cao et al. 2017) had shown that the DM contribution from a pulsar wind is less than $10 \text{ cm}^{-3} \text{ pc}$ for a reasonable range of pair multiplicity parameter. The DM of such origins can be even smaller, as the electrons close to the FRB should be relativistic and contribute little to the DM (Lominadze & Pataraya 1982; Gurevich et al. 2006).

However, optical observations have shown that the repeating FRB 121102 is in a star-forming region (Kokubo et al. 2017; Bassa et al. 2017) and the source DM may not be negligible (Yang et al. 2017). In this paper, we take a least-informative assumption (Jaynes 2003) that DM_{src} follows a uniform PDF in a rather wider range from 0 to $50 \text{ cm}^{-3} \text{ pc}$. In this way, we incorporate the unknowns into the error of inferred parameters.

3.4 The PDF of the FRB host galaxy DM

Xu & Han (2015) have modelled the FRB host DM distribution assuming that the host galaxies are Milky Way-like or M31-like. In our work, we use Monte Carlo simulations to calculate the rest-frame DM distribution function, i.e. the DM distribution function as seen by observers local to the galaxies. Compared with Xu & Han (2015), instead of focusing on specific galaxies, we study the galaxy population and build an ensemble DM PDF. That is, we want to determine how the DM distribution of FRBs looks like for a galaxy-rest-frame observer. The summary for our recipe is as follows:

i) For a given galaxy type, we simulate the H α and r -band luminosity for one galaxy each time according to the galaxy H α and r -band luminosity function (Nakamura et al. 2003, 2004) at the zero redshift. The details are described in Section 3.4.1.

ii) Using the simulated values of H α and r -band luminosity from the step i), we simulate one DM value for an FRB in the galaxy for a rest-frame observer. Here, the DM value is computed by scaling from the ‘template galaxies’, where the DM distribution of template galaxies are calculated in Section 3.4.2. The scaling between the DM_{host} of two galaxies of the same type for the given line of sight depends on the size of the galaxy and electron density, where (see Section 3.4.1),

$$\frac{\text{DM}_{\text{host},1}}{\text{DM}_{\text{host},2}} \propto \sqrt{\frac{L_{\text{H}\alpha,1} R_{\text{e},2}}{L_{\text{H}\alpha,2} R_{\text{e},1}}}. \quad (24)$$

Here, $L_{\text{H}\alpha}$ is the H α luminosity, R_{e} is the effective radius of galaxy being derived from the r -band luminosity.

iii) We repeat the steps ‘i’ and ‘ii’ for one million times and use the accumulated DM values to build the DM distribution function. The analytic form of the distribution function is then derived by curve fitting. The DM distribution function ($f_{\mathcal{D}}(\text{DM}_{\text{host}})$) at this stage is the rest-frame-zero-redshift distribution function, because we compute the DM value for the rest-frame observers using the nearby galaxy luminosity function.

iv) We convert the *rest-frame-zero-redshift* DM distribution function to the *rest-frame* DM distribution function to accommodate the evolution of star formation history. As the H α luminosity scales with the star formation rate (SFR, see Kennicutt et al. 1994; Madau et al. 1998), the electron density n_{e} becomes SFR-dependent that $n_{\text{e}} \propto \text{SFR}^{1/2}$ (see

Appendix D). The rest-frame DM distribution function at redshift z then becomes

$$f_{\mathcal{D}}(\text{DM}_{\text{host}}|z) = \sqrt{\frac{\text{SFR}(0)}{\text{SFR}(z)}} f_{\mathcal{D}} \left[\text{DM}_{\text{host}} \sqrt{\frac{\text{SFR}(0)}{\text{SFR}(z)}} \right], \quad (25)$$

i.e. $f_{\mathcal{D}}(\text{DM}_{\text{host}}|z)$ is the distribution function of DM_{host} at the redshift z measured by the rest-frame observers also at the redshift z . Here the function $f_{\mathcal{D}}[\cdot]$ on the right-hand side of the equation is the zero-redshift-rest-frame DM distribution function from the step iii). The star formation history we used (Hopkins & Beacom 2006) is

$$\text{SFR}(z) = \frac{0.017 + 0.13z}{1 + (z/3.3)^{5.3}} M_{\odot} \text{ yr}^{-1} \text{ Mpc}^{-3}. \quad (26)$$

3.4.1 DM scaling via host galaxy $\text{H}\alpha$ and r -band luminosity

The average electron density is computed from $\text{H}\alpha$ luminosity (Appendix D) with

$$\langle n_e \rangle = 1.0 \eta^{2/3} \left(\frac{T}{10^4 \text{ K}} \right)^{0.45} \left(\frac{L_{\text{H}\alpha}}{10^{40} \text{ erg s}^{-1}} \right)^{1/2} \left(\frac{R}{1 \text{ kpc}} \right)^{-3/2} \text{ cm}^{-3}, \quad (27)$$

where η is the filling factor, T is the ionised gas temperature, and R is the galaxy radius. The typical electron temperatures in galaxies are in a rather narrow range from 5,000 K to 10,000 K. Due to the flat 0.45 index, we fix the gas temperature to 8,000 K, which leads to at most 20% error in determining n_e .

Because $\text{DM}_{\text{host}} \propto n_e R_e$, the scaling relation between the DM_{host} values of two galaxies for the line of sight along the same directions becomes

$$\frac{\text{DM}_{\text{host},1}}{\text{DM}_{\text{host},2}} = \frac{\langle n_e \rangle_1 R_{e,1}}{\langle n_e \rangle_2 R_{e,2}} = \sqrt{\frac{L_{\text{H}\alpha,1} R_{e,2}}{L_{\text{H}\alpha,2} R_{e,1}}}. \quad (28)$$

In this way, once we know the DM value of a template galaxy, we can calculate the DM value of another galaxy of the same type by using the above scaling equation. The unknown filling factor in Equation (27) is canceled, assuming it is a constant for all the galaxies with the same type. The template galaxy is not necessarily a typical member of the given type and merely serves as a reference. We delay the discussions on the template galaxy to the next section, and focus on the distribution functions of $L_{\text{H}\alpha}$ and R_e at the moment.

$L_{\text{H}\alpha}$ is simulated according to the $\text{H}\alpha$ luminosity functions. Based on the complete survey data from the *Sloan Digital Sky Survey* with a redshift depth of $z = 0.12$, Nakamura et al. (2004) measured the morphologically classified $\text{H}\alpha$ luminosity functions. The $\text{H}\alpha$ luminosity functions for the early-type galaxies (ETGs, with morphological index $T_{\text{morph}} \leq 1.0$ as defined by Nakamura et al. 2004) and the later-type galaxies (LTGs, with morphological index

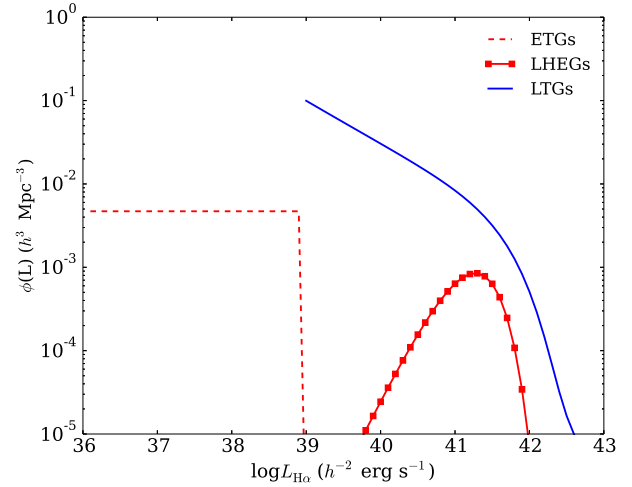


Figure 1. The $\text{H}\alpha$ luminosity functions for ETGs and LTGs. The solid curve (blue) is for the LTG luminosity function. For the luminosity of ETGs, we extended the original results of Nakamura et al. (2004) (in red curve with square marks), where our extension is plotted as the red dashed curve. The details of extension operation are described in the main text.

$T_{\text{morph}} > 1.5$) take forms of

$$\begin{aligned} \phi_{\text{ETG}}(L_{\text{H}\alpha}) &\propto 0.8 \left(\frac{L_{\text{H}\alpha}}{10^{40.02}} \right)^{0.79} e^{-\frac{L_{\text{H}\alpha}}{10^{40.02}}}, \quad (29) \\ \phi_{\text{LTG}}(L_{\text{H}\alpha}) &\propto 1.0 \left(\frac{L_{\text{H}\alpha}}{10^{41.7}} \right)^{-1.4} e^{-\frac{L_{\text{H}\alpha}}{10^{41.7}}} \\ &+ 1.0 \left(\frac{L_{\text{H}\alpha}}{10^{41.7}} \right)^{-1.53} e^{-\frac{L_{\text{H}\alpha}}{10^{41.71}}} \\ &+ 0.01 \left(\frac{L_{\text{H}\alpha}}{10^{42.8}} \right)^{-1.77} e^{-\frac{L_{\text{H}\alpha}}{10^{42.8}}}. \quad (30) \end{aligned}$$

Here we summed the luminosity functions of the sub-types to form the luminosity functions of LTGs. The functions are plotted in Figure 1.

As shown in Figure 1, the ETG $\text{H}\alpha$ luminosity function of Nakamura et al. (2004) peaks around $L = 10^{41} \text{ erg s}^{-1}$. As a common cherished belief (e.g. Kennicutt 1998), most of the ETGs are the old galaxies with little star forming activity and hence with low $\text{H}\alpha$ luminosities. However, the results of Nakamura et al. (2004) indicate that the average $\text{H}\alpha$ luminosity of ETGs would be higher than that of LTGs. Such discrepancy is mainly due to selection effects, that the low $\text{H}\alpha$ luminosity galaxies were invisible in the survey and the *luminous H-alpha elliptical galaxy* (LHEG) contributions start to bias the results. Indeed, Nakamura et al. (2004) mentioned if the sample selection criterion they used is strong enough, they would reject 235 AGNs, which is 35% in the current $\text{H}\alpha$ detected sample including both the ETGs and the LTGs. To compute the missing fraction of ETGs in the $\text{H}\alpha$ selected sample, we compare the $\text{H}\alpha$ luminosity functions with the r -band luminosity functions (Nakamura et al. 2003) of the same sample. The integrated ETG volume density using the r -band luminosity function is $n^* = 2 \times 10^{-2} h^3 \text{ Mpc}^{-3}$, while the galaxy volume density produced by the $\text{H}\alpha$ luminosity

function is only $n^* = 7.2 \times 10^{-4} h^3 \text{Mpc}^{-3}$. Clearly, the majority (more than 90%) of ETGs are below the detection limit in the $\text{H}\alpha$ selection. We thus regard the original $\text{H}\alpha$ luminosity function of ETGs in Nakamura et al. (2004) only applicable for LHEGs.

In order to get the $\text{H}\alpha$ luminosity distribution for the full ETG population, an extension operation is needed. As little information is available for these low $\text{H}\alpha$ luminosity galaxies, we perform the most naïve correction. We assume that the missing ETGs distribute uniformly in logarithmic luminosity space below the survey sensitivity. Such an extension scheme introduces the least amount of information as being widely applied in the Bayesian statistics (Jaynes 2003). The extension leads to a constant density $\phi = 4.7 \times 10^{-3} h^3 \text{Mpc}^{-3}$ in the range of $10^{36} \text{erg s}^{-1} < L < 10^{39} \text{erg s}^{-1}$.

We now turn to the distribution of galaxy radii. The galaxy radius can be calculated from the optical luminosity using empirical size-magnitude relations (Shen et al. 2003), that

$$\log\left(\frac{\bar{R}_{50}}{\text{kpc}}\right) = \begin{cases} -0.4aM + b, & \text{for ETGs} \\ -0.4\alpha M + (\beta - \alpha) \log[1 + 10^{-0.4(M-M_0)}] \\ +\gamma, & \text{for LTGs.} \end{cases} \quad (31)$$

We sample the r -band optical magnitude (M) based on the luminosity functions of Nakamura et al. (2003) and use the above size-magnitude relations to compute the Petrosian half-light radius (R_{50} , see Petrosian 1976), where constants $a = 0.60$, $b = -4.63$ for ETGs and $\alpha = 0.21$, $\beta = 0.53$, $\gamma = -1.31$, $M_0 = -20.52$ for LTGs. We then convert the Petrosian radius to the effective radius (Graham et al. 2005), that, for ETGs $R_{50} = 0.73 R_e$, and, for LTGs $R_{50} = 0.99 R_e$.

To confirm the validity of above modelling, we compare the estimated values with the observations. For the LTG, the measured stellar-density-weighted electron density of the Milky Way by the YMW16 is $\langle n_e \rangle = 0.04 \text{cm}^{-3}$, while the current modelling ($R_e \approx 3.5 \text{kpc}$, $L_{\text{H}\alpha} \approx 5 \times 10^{40} \text{erg s}^{-1}$) produces $0.014 \sim 0.066 \text{cm}^{-3}$ when we adopt the filling factor from 0.01 to 0.1. For the ETG type, the measured average free electron density of M87 from Chandra observations (Cavagnolo et al. 2009) is $\langle n_e \rangle = 0.05 \text{cm}^{-3}$, and the modelled electron density ($R_e \approx 7.7 \text{kpc}$, $L_{\text{H}\alpha} = 10^{40} \text{erg s}^{-1}$) is $0.009 \sim 0.042 \text{cm}^{-3}$. Clearly, the predictions for the electron density depend on the filling factor. However, since we are using the scaling relation, Equation (28), to compute the DM of the simulated galaxies, the filling factors cancel out. In this case, the results will not be affected.

As a short summary for this section, we create a large sample of artificial galaxies, in which $L_{\text{H}\alpha}$ follows the morphological luminosity function (Equation (29) or (30)) and radius follows the size distribution in Equation (31). We then convert the DM_{host} of a template galaxy (see below in 3.4.2) to that of the given galaxy according to Equation (28). The DM distribution of the template galaxies and galaxy ensembles will be discussed in the next section.

3.4.2 DM for the template galaxies

In this section, we compute the DM distribution of the template galaxies, where the stellar distribution and electron density modelling of galaxies are considered. Due to the mor-

phological difference, we need to address the ETGs, LHEGs, and the LTGs separately.

ETGs and LHEGs: The electron density model of ETGs, unfortunately, is not well studied statistically, particularly due to the low gas fraction. Also one usually needs galaxies with larger angular diameters, that can be resolved in order to measure the electron distribution. As a result, there will be only a few ETGs with electron density profile measurements, and those ETGs might not fall into the class of stereotype. However, as explained above, since our DM scaling relation accounts for both galaxy size and luminosity, we can use any individual member as the reference. As a caveat, we need to assume that the gas filling factor varies only mildly in the galaxy population. In the paper, M87 is chosen as the reference, simply because it has a published electron density profile (Cavagnolo et al. 2009).

The electron density profile of M87 derived from Chandra surface brightness measurements (Cavagnolo et al. 2009) can be characterised by the following function (Fabricant & Gorenstein 1983)

$$n_e = n_0 \left[1 + \left(\frac{R}{R_0} \right)^2 \right]^{\alpha_e}, \quad (32)$$

where the fitted parameters are $n_0 \approx 0.165 \text{cm}^{-3}$, $R_0 = 1.544 \text{kpc}$, and $\alpha_e = -0.582$.

We calculate the DM PDF of FRBs in the M87 using the Monte Carlo method. First, we create the a million artificial FRBs with positions according to the Young profile (Young 1976)

$$\rho_s = \rho_0 \frac{\exp\left[-b(R/R_e)^{1/4}\right]}{(R/R_e)^{7/8}}, \quad (33)$$

where ρ_0 is the stellar density and $R_e = 7.7 \text{kpc}$ for M87 (Zeilinger et al. 1993). We then compute the DM PDF of those FRBs by integrating the electron density (i.e. Equation (32)) along the path in random directions uniformly distributed over the full-sky 4π solid angle. The DM PDF is plotted in Figure 2.

The DM distribution function of M87 is rather flat, due to the spherical electron density distribution. The FRBs in ETGs is concentrated around the galaxy centre, because of the rather compact Young profile. For the case of M87, the little spike in the DM distribution function peaking around $600 \text{cm}^{-3} \text{pc}$ is due to such a concentration. M87 is a giant elliptical galaxy, the high DM value with a few hundred $\text{cm}^{-3} \text{pc}$ comes as no surprise. For most of the ETGs, we expect that the DM will be much lower, because of their smaller sizes and lower $\text{H}\alpha$ luminosities.

Fixing the M87 as the reference galaxy, we compute the DM distribution function for all ETGs with another Monte Carlo simulation. In each step, we draw one sample of DM value from the M87 distribution, $\text{H}\alpha$ luminosity from luminosity function, and R_e via r -band luminosity function. Then, we use Equation (28) to compute the DM of the simulated galaxy. We repeat the procedures and produce the DM distributions of ETGs and LHEGs, which are plotted in Figure 3.

For reference purposes, we approximate the DM distribution using an analytical form. We note that the double-

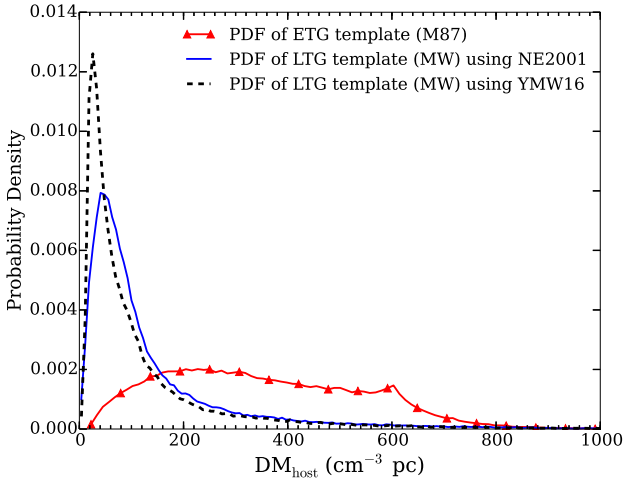


Figure 2. The DM distribution of the reference galaxies, i.e. for the Milky Way and the M87. The solid curve with triangle marks (red) is PDF of DMs of FRBs in the M87. The solid curve (blue) and the dashed curve (black) are for the Milky Way using the NE2001 model and the YMW16 model, respectively.

Gaussian function, i.e.

$$f_{\mathcal{D}}(\text{DM}_{\text{host},0}) d\text{DM}_{\text{host},0} = \sum_{i=1}^2 a_i e^{-\left(\frac{\log_{10} \text{DM}_{\text{host},0} - b_i}{c_i}\right)^2} d\text{DM}_{\text{host},0}. \quad (34)$$

can fit the curves rather well. The fitted parameters and the curves for those ensemble DM distribution functions are listed in Table 2 and shown in Figure 3 respectively.

LTGs: We adopt Milky Way as the reference galaxy for the LTGs. The Milky-Way stellar structure can be well approximated by the combination of a thin exponential disk and a Young-profile spheroid. We use the BS model (Bahcall & Soneira 1980, 1984; Bahcall 1986) and the Young profile, i.e. Equation (33), to model the stellar distribution. The stellar distribution of the disk component is

$$\rho_{\text{D}}(\varpi, Z) = \rho_{\text{D0}} \exp\left[-\frac{Z}{H^*}\right] \exp\left[-\frac{\varpi - \varpi_0}{\varpi^*}\right], \quad (35)$$

where the radial distance to the Z -axis is $\varpi = \sqrt{X^2 + Y^2}$. The central stellar density $\rho_{\text{D0}} = 0.13 \text{ pc}^{-3}$, $\varpi_0 = 8 \text{ kpc}$, scale height $H^* = 0.3 \text{ kpc}$, and scale radius $\varpi^* = 3.5 \text{ kpc}$. For the spheroid component, the density profile is described by the Young profile as in Equation (33), with $\rho_0 = 2.6 \times 10^{-4} \text{ pc}^{-3}$, $R_e = 2.7 \text{ kpc}$, and $b \simeq 7.7$.

The electron density models we used are the NE2001 and the YMW16. The simulated DM distribution for Milky Way is plotted in Figure 2. The DM distribution function of the LTG template is relatively compact compared to the case of the ETG template, because LTGs have an exponential drop of the stellar distribution and the electron density distribution in both radial and vertical directions of the disk component. The most probable DM values are 40 and 25 $\text{cm}^{-3} \text{ pc}$ for the NE2001 and the YMW16 model, respectively, which are a factor of 3 to 4 smaller than previous estimations (Thornton et al. 2013). Using the same method described for ETGs, we compute the ensemble distribution

functions of LTGs. The DM distribution is shown in Figure 3, and the fitted results are in Table 2.

All galaxies: We can combine the ETGs and LTGs to form the total galaxy population and define the sample as “all galaxies” (ALGs). The integrals of the r -band luminosity functions (Nakamura et al. 2003) produce the fraction number of ETGs and LTGs, which are 23.7% and 76.3%, respectively. Due to the dominance of LTGs, the DM distribution function of ALGs is very similar to that of LTGs. The results are shown in Figure 3 and Table 2.

With the DM_{host} distribution, the most probable isotropic luminosity and energy of FRB emission can be estimated as the byproducts. The technique is described in Appendix F and the results are given in Table B1.

3.5 Posterior sampling and algorithm verification

Our likelihood is given in Equation (19). Choosing the uniform prior for the dimensionless parameters and the uniform prior in logarithmic scale for the parameters with units introduces the least amount of prior information (Gregory 2005). We thus choose uniform prior for α and $\log L^*$. However, as we will show, we can not measure the lower cutoff of FRB luminosity L_0 yet, due to the limited FRB sample. The standard trick to determine the upper limit (Lentati et al. 2015) is to use the uniform prior for L_0 .

Instead of a direct evaluation for the integration in Equation (4), the posterior calculation is usually performed using sampling techniques. In this paper, we use the MULTINEST algorithm (Feroz et al. 2009), which is widely applied in astronomical applications. The nested sampling (Skilling 2004) is a Monte Carlo method to compute Bayesian evidence efficiently and produce the posterior samples. This is done by converting the parameter space to a set of nested shells with equal posterior values and iteratively sampling with replacements in the nested volume. To achieve a better efficiency, MULTINEST further partitions the nested samples. In our posterior sampling, we use the python language interface PYMULTINEST² when calling the MULTINEST library.

We test the likelihood function, prior choice, and MULTINEST sampler using the simulated mock data set. The mock data is generated by (1) sampling the luminosity of FRB according to the input FRB luminosity function; (2) sampling the FRB redshift according to Equation (20); (3) sampling the host galaxy DM for fixed galaxy type according to the distribution function in Equation (34); (4) sampling the local DM according to uniform probability distribution mentioned in Section 3.3; (5) sampling beam response according to the distribution mentioned in Section 3.2; (6) calculating the FRB flux density and extragalactic DM; and (7) selecting the sources above the detection threshold.

The results from analysing the mock data are shown in Figure 4. As one can see, the current Bayesian inference recovers the parameters of the input luminosity function rather well.

² <https://johannesbuchner.github.io/PyMultiNest/>

Table 2. The fitted parameters of DM PDF

Parameters	ETGs	LHEGs	LTGs(NE2001)	LTGs(YMW16)	ALGs(NE2001)	ALGs(YMW16)
$a_1(\times 10^{-3})$	1.963	0.1182	14.31	17.51	4.899	13.79
b_1	1.099	3.441	1.062	0.759	0.8665	0.7597
c_1	0.2965	0.4407	0.5202	0.3013	1.009	0.3082
$a_2(\times 10^{-3})$	14.28	0.09462	3.471	21.19	12.56	19.96
b_2	1.055	2.906	0.7227	1.042	1.069	1.048
c_2	0.7262	0.5317	1.151	0.5791	0.5069	0.6025

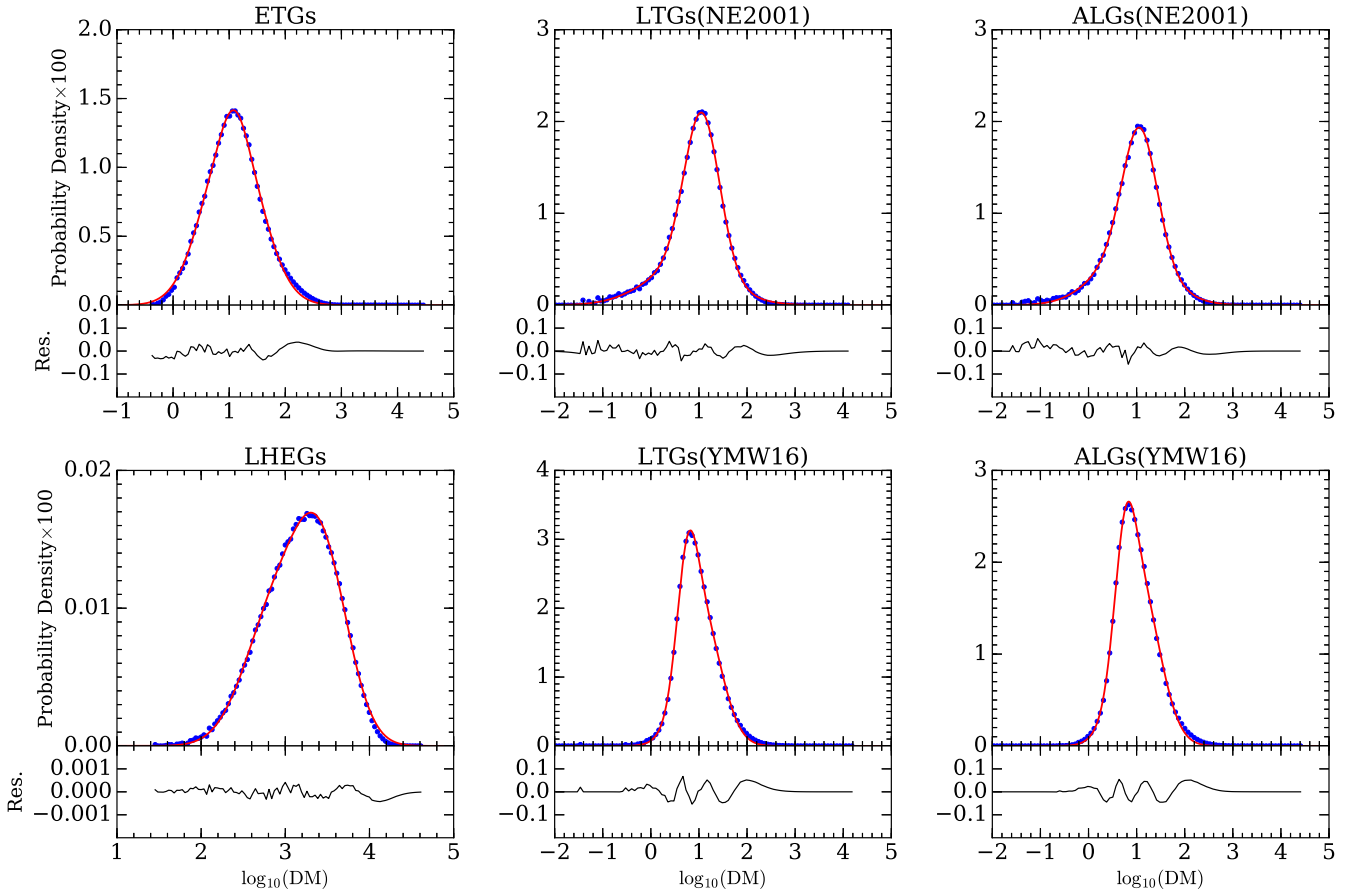


Figure 3. The DM distribution functions and the fitted functions before normalisation. Here are six galaxy categories: early-type galaxies (ETGs), luminous H α elliptical galaxies (LHEGs), late-type galaxies (LTGs), and all galaxies (ALGs) using two different electron density models: NE2001 and YMW16. The recipe to compute the curves is in Section 3.4. For each panel, the galaxy type and electron density model are given in the title. The simulated DM distribution function using Monte Carlo method is plotted in blue dots. The fitted curve is plot as the red curves, with residuals in the bottom panels.

4 RESULTS FOR THE FRB LUMINOSITY FUNCTION

We perform our Bayesian inference and use the data of 33 FRBs to measure the FRB luminosity functions for the following six cases.

Case 1, ETG-NE2001 Host galaxy is assumed as ETGs, and NE2001 electron model is assumed for Galactic DM correction.

Case 2, ETG-YMW16 The same as the **Case 1**, except using YMW16 to correct the Galactic DM.

Case 3, LTG-NE2001 The same as the **Case 1**, except that the host galaxy is assumed as LTGs.

Case 4, LTG-YMW16 The same as the **Case 2**, except that the host galaxy is assumed as LTGs.

Case 5, ALG-NE2001 The same as the **Case 1**, except that the host galaxy is assumed as the composition of both LTGs and ETGs.

Case 6, ALG-YMW16 The same as the **Case 2**, except that the host galaxy is assumed as the composition of both LTGs and ETGs.

The plots for posterior PDF of all six cases are sum-

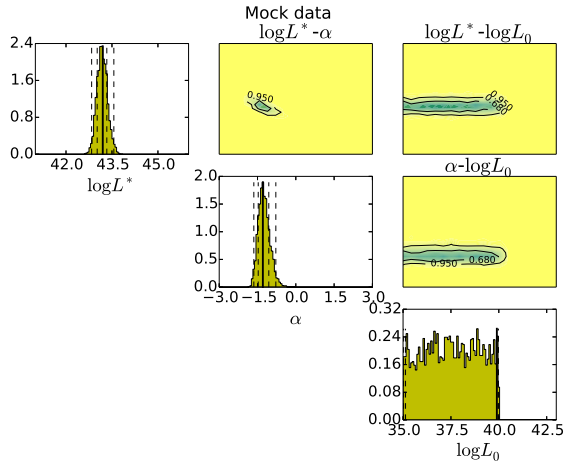
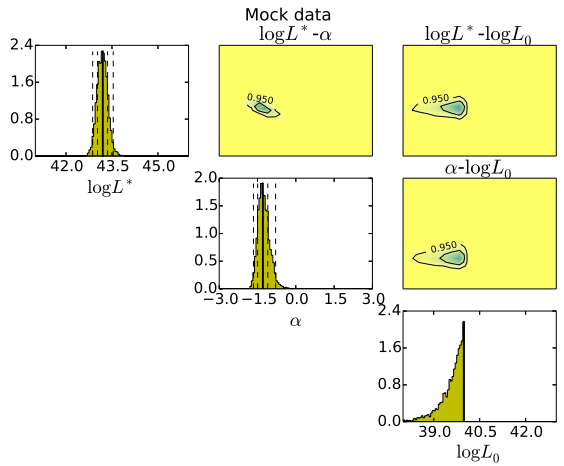
(a) Posterior distribution using uniform prior for $\log L_0$ (b) Posterior distribution using uniform prior for L_0

Figure 4. Inference for the mock data. The parameters used in creating the mock data are $\log L^* = 43.0$, $\alpha = -1.0$, and $\log L_0 = 39.0$. The diagonal histogram is the marginalised one-dimensional posterior distribution for each of the parameters. For $\log L^*$ and α , the solid lines denote the most probable parameter value, while the dashed lines indicate the 67% and the 95% confidence level. For $\log L_0$, the solid line denote the upper limit value with 95% confidence level. The off-diagonal contour plots are for the marginalised two-dimensional posteriors, with parameters indicated in the title. The inner and outer black contours are for 67% and 95% confidence levels. In the panel (a), we adopt uniform prior for $\log L_0$. As indicated by the flat histogram of the $\log L_0$ distribution, we can not get good measurement for the value of L_0 . This is mainly due to the limited number sample (100 FRBs are simulated here). We switch the uniform prior for L_0 to produces the upper limit of L_0 , as shown in the panel (b).

marised in Appendix G. The maximal likelihood estimators and the errors are summarised in Table 3. For each of the six cases, we compared two scenarios, i.e. removing the Galactic halo contributions DM_{halo} or not in the pre-processing stage. The shapes of luminosity functions together with the confidence regions are plotted in Figure 5. Interestingly, even though the DM distribution functions depend on the galaxy types, the inferred luminosity functions do not vary much, where the power-law index $\alpha \approx -1.5$ and cut-off luminosity

$\log L^* \approx 44.2$. We can not measure the low cut-off luminosity $\log L_0$ due to the limited number of currently known FRBs, however the 95%-confidence-level upper limit $\log L_0 \leq 41.9$ is derived with a uniform prior for L_0 .

5 DISCUSSION

In this paper, we measured the FRB luminosity function using the Bayesian method under different assumptions for the host galaxy type. The Bayesian method helped dealing with the missing information, i.e. the distances of FRBs and beam response, which are difficult to handle otherwise. Assuming the Schechter form for the luminosity function, we measured the power law index and high cut-off luminosity, where $\alpha \approx -1.5$, and $L^* \approx 10^{44} \text{ erg s}^{-1}$. As byproducts, we also used the Bayesian method (see Appendix F) to infer the most-probable redshift, isotropic luminosity and energy of each source with the values listed in Appendix B.

The FRB luminosity power-law indices, we measured, range from -1.8 to -1.2 . Such values also agree with (i) the power-law indices of pulsars' giant pulse flux distribution at lower frequency (-1.7 , Karuppusamy et al. 2012); (ii) the mean power-law indices of radio emission of pulsars (-1.65 to -2.2 , Han et al. 2016; Jankowski et al. 2018); (iii) the power-law index of luminosity function of long gamma-ray bursts (-1.3 to -2.3 ; Sun et al. 2015; Pescalli et al. 2016) (iv) short gamma-ray bursts (-1.5 to -1.7 , Sun et al. 2015); (v) compact binary mergers (-1.2 to -1.7 , Cao et al. 2018). We can not pin down the radiation mechanisms based on the FRB luminosity function. However, the similarity between it and those of other astrophysical sources may suggest a common underlying rule of defining burst populations of different kinds.

The distance information of FRBs is determined from the DM values. We modelled the DM from three major contributions, i.e. from the Milky way, the IGM, and the FRB host galaxy. We also compared the results to evaluate the effects of Galaxy halo contribution. We showed that the parameters for the luminosity function are rather insensitive to the modeling details.

We modelled the electron density distribution functions for two major cases in the paper, i.e. spiral galaxies and elliptical galaxies. The most likely values of DM_{host} for these two cases are approximately 10 and $15 \text{ cm}^{-3} \text{ pc}$, respectively. Such host galaxy DM values are at least one order of magnitude smaller than that of the IGM contribution. Although the most uncertain part in our modelling is the DM_{host} distribution, the parameters inference for the luminosity function is rather robust as $DM_{\text{E}} \gg DM_{\text{host}}$. We can tolerate the missing information such as the the $H\alpha$ filling factor, the stellar distribution in galaxies, halo DM or FRB source DM. The characteristic host galaxy DM values we estimated are less than $100 \text{ cm}^{-3} \text{ pc}$. Despite this, considering the scattering of the distribution, our results are still compatible with the values estimated before (Thornton et al. 2013; Xu & Han 2015; Yang et al. 2017).

The average DM value of ETGs we calculated here is higher than that for LTGs. This is mainly due to the stellar distribution and galaxy morphology. The concentration of FRBs in the central region of ETGs produce higher value

Table 3. The parameters of FRB luminosity function

Galaxy type	No modelling for Galactic halo			Removed Galactic halo		
	$\alpha (1\sigma)$	$\log L^* (1\sigma)$	$\log L_0$ (95% C.L.)	$\alpha (1\sigma)$	$\log L^* (1\sigma)$	$\log L_0$ (95% C.L.)
ETGs (NE2001)	$-1.52^{+0.24}_{-0.23}$	$44.14^{+0.23}_{-0.33}$	≤ 41.75	$-1.57^{+0.19}_{-0.26}$	$44.10^{+0.23}_{-0.33}$	≤ 41.56
ETGs (YMW16)	$-1.62^{+0.29}_{-0.21}$	$44.18^{+0.26}_{-0.38}$	≤ 41.96	$-1.67^{+0.21}_{-0.25}$	$44.23^{+0.27}_{-0.38}$	≤ 41.82
LTGs (NE2001)	$-1.45^{+0.31}_{-0.28}$	$43.94^{+0.22}_{-0.35}$	≤ 41.74	$-1.50^{+0.25}_{-0.26}$	$43.87^{+0.27}_{-0.30}$	≤ 41.56
LTGs (YMW16)	$-1.57^{+0.17}_{-0.27}$	$44.32^{+0.22}_{-0.24}$	≤ 41.96	$-1.60^{+0.15}_{-0.19}$	$44.29^{+0.33}_{-0.20}$	≤ 41.82
ALGs (NE2001)	$-1.42^{+0.27}_{-0.27}$	$43.90^{+0.30}_{-0.29}$	≤ 41.74	$-1.51^{+0.26}_{-0.25}$	$43.89^{+0.26}_{-0.28}$	≤ 41.56
ALGs (YMW16)	$-1.57^{+0.19}_{-0.21}$	$44.31^{+0.22}_{-0.27}$	≤ 41.96	$-1.63^{+0.16}_{-0.19}$	$44.34^{+0.21}_{-0.29}$	≤ 41.82

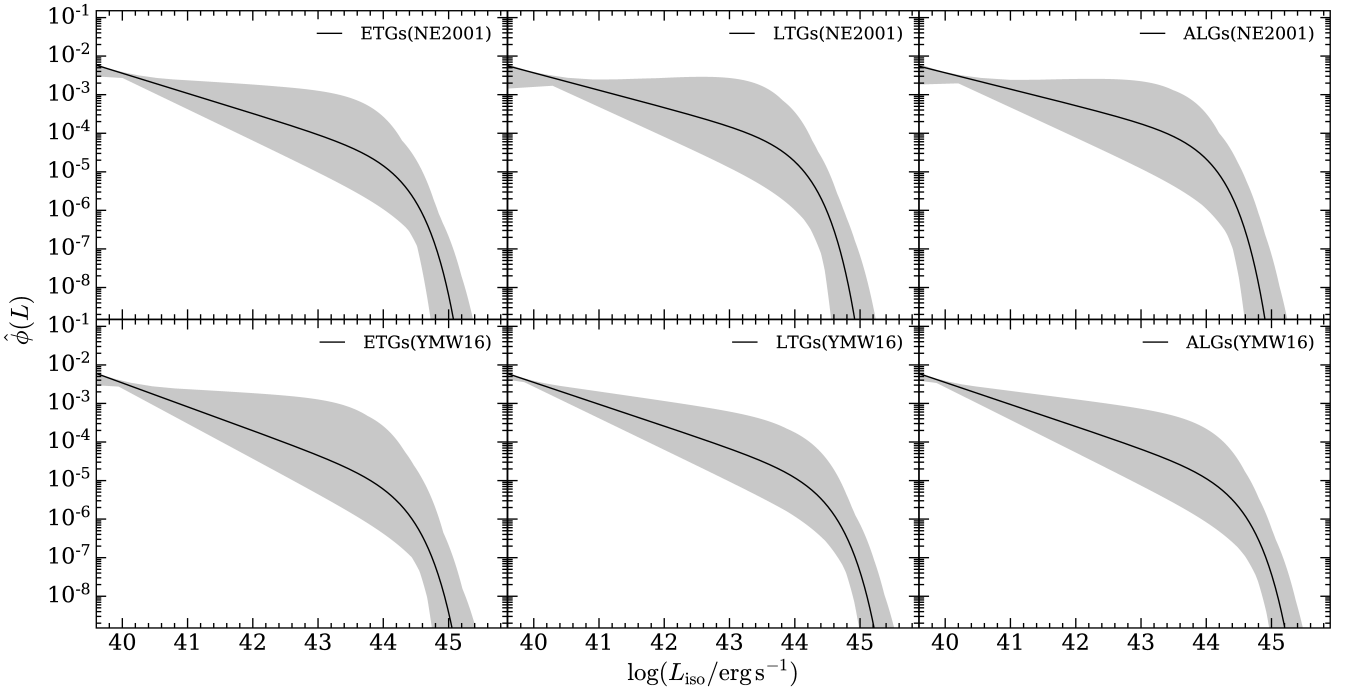


Figure 5. The FRB normalised luminosity functions. In each panel, the solid line (black) is the best fitting luminosity function, and the shaded area (grey) shows the luminosity function within 1σ error. The meaning of the labels are, 1° ETGs(NE2001): Galactic foreground removed with NE2001 and assuming ETG as the host galaxy; 2° ETGs(YMW16): the same as 1° but with galactic foreground removed with YMW16; 3° LTGs(NE2001): Galactic foreground removed with NE2001 and assuming LTG as the host galaxy; 4° LTGs(YMW16): the same as 3° but with galactic foreground removed with YMW16; 5° ALGs(NE2001): Galactic foreground removed with NE2001 and assuming mixed galaxy (ALG) as the host galaxy; 6° ALGs(YMW16): the same as 5° but with galactic foreground removed with YMW16.

of DM for the ETGs than for the LTG, where a lower scale height of LTGs leads to a lower DM.

For the case of LHEGs, i.e. elliptical galaxies with $H\alpha$ luminosity function in Nakamura et al. (2004), the most likely DM host is $DM_{\text{host}} \approx 3000 \text{ cm}^{-3} \text{ pc}$. Considering that the observed DM_{host} is smaller by a factor $(1+z)$ and the roughly linear increase of DM_{IGM} with redshift, one obtains that an FRB with $z > 2$ would have a DM_{E} exceeding $2750 \text{ cm}^{-3} \text{ pc}$ (Zhang 2018a) which is larger than the maximum observed DM_{E} (e.g. $2583.1 \text{ cm}^{-3} \text{ pc}$ from FRB 160102, Bhandari et al. 2018). If FRBs all have LHEG hosts, the probability of detecting one FRB with $DM_{\text{E}} \leq 2750$ is only $\approx 35\%$, as computed by integrating $f_{\mathcal{D}}(DM_{\text{host}})$ from 0 to 2750. Thus there is only a minuscule chance (8×10^{-16}) to observe all 33 FRBs with $DM_{\text{E}} \leq 2750 \text{ cm}^{-3} \text{ pc}$. We conclude that it is unlikely

that the LHEGs are the host galaxies for FRBs, unless all FRBs lie around the galaxy outskirts if they originate in LHEGs.

The DM_{host} distribution function of all the galaxies enables us to infer the corresponding isotropic luminosity and energy of FRB emission as listed in Table B1. Using only DM as the distance indicator, our inferred most probable redshift of FRB 121102 ranges from 0.198 to 0.271 at a 2σ confidence level. This is roughly consistent with the true redshift 0.193 (Tendulkar et al. 2017). The slightly higher value of the inferred redshift may be resulted from the long tail of PDF for DM_{host} as computed in Section 3.4. The excess may also come from an underestimate of the electron density in the Milky Way halo or in the FRB environment. Alternatively, it could be due to the deviation of the mean

cosmological DM_{IGM} due to the existence of large scale structures, so that the line of sight towards FRB 121102 may have pieced through an over-dense region in the IGM. We expect that more FRBs with optically-measured redshift will help us to clarify these issues.

We used M87 and Milky Way as the template galaxies in this study. The choice is made because they are the only two galaxies of each type that previously have accurate measurements on both electron density distributions and $H\alpha$ luminosities. As a caveat, both galaxies may not be the typical example of ETGs or LTGs. The M87 is a giant elliptical galaxy, and the Milky way has a relatively low gas fraction (Kennicutt & Evans 2012). We can still use Milky Way and M87 as the reference values, thanks to our scaling method, which accounts for the galaxy size, electron density, and star formation history evolution.

We assumed that the FRB distribution in the galaxies follows the stellar distribution. In Milky Way, the stellar distribution has low scale height than that of the neutron star distribution. If the FRBs are of a magnetar or pulsar origin, the host galaxy DM may be slightly overestimated here. However, since the host galaxy DM is already smaller than the observed DM, such a second-order small perturbation can be well neglected without affecting the luminosity function inference.

We modelled the luminosity distribution using the Schechter function. The measured cut-off luminosity $\log L^* \simeq 44.2 \text{ erg s}^{-1}$ with an error of 0.3 dex indicates that the simple power-law distribution is not precise enough at the high luminosity end. This also helps planning future FRB surveys. For FRBs with distances of $\sim 1 \text{ Gpc}$, the size of a radio telescope for FRB survey should be at least 10 meters to get $S/N \geq 7$.

The possible off-centre position of an FRB in the main beam, without modelling, leads to an underestimate for the FRB luminosity (Niino 2018). We include such an uncertainty through the Bayesian marginalisation. It turns out that the difference in the parameters of inferred luminosity function is not significant between the two cases, regardless of whether or not the beam response is taken into account. Without modelling the beam response, the power-law index of Schechter function is slightly flatter, and the cut-off luminosity is relatively lower. Taking the case of ALGs-YMW16 as an example, we get $\alpha = -1.56^{+0.21}_{-0.20}$ and $\log L^* = 44.19^{+0.22}_{-0.24}$ with no beam response modelling, whereas $\alpha = -1.57^{+0.19}_{-0.21}$ and $\log L^* = 44.31^{+0.22}_{-0.27}$ with beam response marginalisation. As the difference is still within 1σ confidence level, we conclude that the beam response plays a limited role in parameter inference for the current limited sample of FRBs.

We could only obtain the upper limits of the lower cut-off luminosity, i.e. L_0 , due to the limited sample of FRBs (Table 3). The current upper limit of $\log L_0 < 42.0$ is not capable of testing the FRB model yet. In order to measure the true value of L_0 , a large number of nearby FRBs are required.

Due to the unknown spectral shape and width, our luminosity function is based on the reference bandwidth of 1 GHz. This is motivated by the observations of the repeating FRB 121102, which indicates a $\sim 1 \text{ GHz}$ bandwidth (Gajjar et al. 2018). In general, the parameter L^* in the luminosity function scales with the reference bandwidth. The

assumption of a $\sim 1 \text{ GHz}$ bandwidth can be revised later. Little information is available for the spectrum of FRBs at present, and scintillation may introduce a strong bias in determining the true bandwidth. The measurement in this paper can be further improved, if future observations will provide more information. We expect that the upcoming large field-of-view facilities, e.g. CHIME (Ng et al. 2017), ASKAP (Macquart et al. 2010), MeerKAT (Booth & Jonas 2012) and instruments with higher sensitivity, e.g. ALFABURST survey (Foster et al. 2017), FAST (Nan et al. 2011), SKA (Macquart et al. 2015), and QTT (Wang 2017), will provide more opportunities to detect more nearby FRBs and reveal the details of the FRB spectra.

ACKNOWLEDGEMENTS

This work was supported by NSFC U15311243 National Basic Research Program of China, 973 Program, 2015CB857101, XDB23010200, 11690024, 11373011, and funding from TianShanChuangXinTuanDui and the Max-Planck Partner Group. We are grateful to Luis C. Ho, Joris P. W. Verbiest and Yuan-pei Yang for reading through the paper and giving their helpful suggestions and comments.

REFERENCES

- Bahcall J. N., 1986, *ARA&A*, **24**, 577
- Bahcall J. N., Soneira R. M., 1980, *ApJS*, **44**, 73
- Bahcall J. N., Soneira R. M., 1984, *ApJS*, **55**, 67
- Bannister K. W., et al., 2017, *ApJ*, **841**, L12
- Bassa C. G., et al., 2017, *ApJ*, **843**, L8
- Bhandari S., et al., 2018, *MNRAS*, **475**, 1427
- Binggeli B., Sandage A., Tammann G. A., 1988, *ARA&A*, **26**, 509
- Bonetti L., Ellis J., Mavromatos N. E., Sakharov A. S., Sarkisyan-Grinbaum E. K., Spallicci A. D. A. M., 2016, *Physics Letters B*, **757**, 548
- Bonetti L., Ellis J., Mavromatos N. E., Sakharov A. S., Sarkisyan-Grinbaum E. K., Spallicci A. D. A. M., 2017, *Physics Letters B*, **768**, 326
- Booth R. S., Jonas J. L., 2012, *African Skies*, **16**, 101
- Born M., Wolf E., eds, 1999, *Principles of optics : electromagnetic theory of propagation, interference and diffraction of light*. Cambridge University Press, New York
- Bregman J. N., Lloyd-Davies E. J., 2007, *ApJ*, **669**, 990
- Burke-Spolaor S., Bannister K. W., 2014, *ApJ*, **792**, 19
- Cai Y.-F., Sabancilar E., Vachaspati T., 2012a, *Phys. Rev. D*, **85**, 023530
- Cai Y.-F., Sabancilar E., Steer D. A., Vachaspati T., 2012b, *Phys. Rev. D*, **86**, 043521
- Caleb M., et al., 2017, *MNRAS*, **468**, 3746
- Cao X.-F., Yu Y.-W., Dai Z.-G., 2017, *ApJ*, **839**, L20
- Cao X.-F., Yu Y.-W., Zhou X., 2018, *ApJ*, **858**, 89
- Cavagnolo K. W., Donahue M., Voit G. M., Sun M., 2009, *ApJS*, **182**, 12
- Champion D. J., et al., 2016, *MNRAS*, **460**, L30
- Chatterjee S., et al., 2017, *Nature*, **541**, 58
- Chennamangalam J., Lorimer D. R., Mandel I., Bagchi M., 2013, *MNRAS*, **431**, 874
- Connor L., Sievers J., Pen U.-L., 2016, *MNRAS*, **458**, L19
- Cordes J. M., Lazio T. J. W., 2002, *ArXiv Astrophysics e-prints*,
- Cordes J. M., Wasserman I., 2016, *MNRAS*, **457**, 232
- Dai Z. G., Wang J. S., Wu X. F., Huang Y. F., 2016, *ApJ*, **829**, 27
- Deng W., Zhang B., 2014, *ApJ*, **783**, L35
- Dolag K., Gaensler B. M., Beck A. M., Beck M. C., 2015, *MNRAS*, **451**, 4277
- Fabricant D., Gorenstein P., 1983, *ApJ*, **267**, 535
- Falcke H., Rezzolla L., 2014, *A&A*, **562**, A137
- Fan X., Carilli C. L., Keating B., 2006, *ARA&A*, **44**, 415
- Farah W., et al., 2017, *The Astronomer's Telegram*, **10697**
- Farah W., et al., 2018, *MNRAS*, **478**, 1209
- Feroz F., Hobson M. P., Bridges M., 2009, *MNRAS*, **398**, 1601
- Fisz M., 1963, *Probability theory and mathematical statistics*, 3 edn. Hohn Wiley & Sons, Inc, New York, NY, USA
- Foster G., et al., 2017, preprint, ([arXiv:1710.10806](https://arxiv.org/abs/1710.10806))
- Fukugita M., Hogan C. J., Peebles P. J. E., 1998, *ApJ*, **503**, 518
- Gaensler B. M., Madsen G. J., Chatterjee S., Mao S. A., 2008, *Publ. Astron. Soc. Australia*, **25**, 184
- Gajjar V., et al., 2018, preprint, ([arXiv:1804.04101](https://arxiv.org/abs/1804.04101))
- Gao H., Li Z., Zhang B., 2014, *ApJ*, **788**, 189
- Geng J. J., Huang Y. F., 2015, *ApJ*, **809**, 24
- Ghisellini G., 2017, *MNRAS*, **465**, L30
- Graham A. W., Driver S. P., Petrosian V., Conselice C. J., Bershadsky M. A., Crawford S. M., Goto T., 2005, *AJ*, **130**, 1535
- Gregory P. C., 2005, *Bayesian Logical Data Analysis for the Physical Sciences: A Comparative Approach with 'Mathematica' Support*. Cambridge University Press
- Gu W.-M., Dong Y.-Z., Liu T., Ma R., Wang J., 2016, *ApJ*, **823**, L28
- Gurevich A. V., Beskin V. S., Istomin Y. N., 2006, *Physics of the Pulsar Magnetosphere*. Cambridge, UK: Cambridge University Press
- Han J., Wang C., Xu J., Han J.-L., 2016, *Research in Astronomy and Astrophysics*, **16**, 159
- Hopkins A. M., Beacom J. F., 2006, *ApJ*, **651**, 142
- Igoshev A., Verbunt F., Cator E., 2016, *A&A*, **591**, A123
- Inoue S., 2004, *MNRAS*, **348**, 999
- Ioka K., 2003, *ApJ*, **598**, L79
- Iwazaki A., 2015, *Phys. Rev. D*, **91**, 023008
- Jankowski F., van Straten W., Keane E. F., Bailes M., Barr E. D., Johnston S., Kerr M., 2018, *MNRAS*, **473**, 4436
- Jaynes E. T., 2003, *Probability Theory: The Logic of Science* (Vol 1). Cambridge Univ. Press, Cambridge, UK
- Karuppusamy R., Stappers B. W., Lee K. J., 2012, *A&A*, **538**, A7
- Kashiyama K., Ioka K., Mészáros P., 2013, *ApJ*, **776**, L39
- Katz J. I., 2016, *ApJ*, **826**, 226
- Katz J. I., 2017, *MNRAS*, **471**, L92
- Keane E. F., Kramer M., Lyne A. G., Stappers B. W., McLaughlin M. A., 2011, *MNRAS*, **415**, 3065
- Keane E. F., Stappers B. W., Kramer M., Lyne A. G., 2012, *MNRAS*, **425**, L71
- Keane E. F., et al., 2016, *Nature*, **530**, 453
- Kelly B. C., Fan X., Vestergaard M., 2008, *ApJ*, **682**, 874
- Kennicutt Jr. R. C., 1998, *ARA&A*, **36**, 189
- Kennicutt R. C., Evans N. J., 2012, *ARA&A*, **50**, 531
- Kennicutt Jr. R. C., Tamblyn P., Congdon C. E., 1994, *ApJ*, **435**, 22
- Kokubo M., et al., 2017, *ApJ*, **844**, 95
- Landau L. D., Lifshitz E. M., 1960, *Electrodynamics of continuous media*. Oxford: Pergamon Press
- Lentati L., et al., 2015, *MNRAS*, **453**, 2576
- Liu T., Romero G. E., Liu M.-L., Li A., 2016, *ApJ*, **826**, 82
- Loeb A., Shvartzvald Y., Maoz D., 2014, *MNRAS*, **439**, L46
- Lominadze J. G., Patariaia A. D., 1982, *Physica Scripta Volume T*, **2**, 215
- Lorimer D. R., Kramer M., 2012, *Handbook of Pulsar Astronomy*. Cambridge University Press, Cambridge, UK
- Lorimer D. R., Bailes M., McLaughlin M. A., Narkevic D. J., Crawford F., 2007, *Science*, **318**, 777
- Lu W., Kumar P., 2018, *MNRAS*, **477**, 2470
- Lynden-Bell D., 1971, *MNRAS*, **155**, 95
- Lyubarsky Y., 2014, *MNRAS*, **442**, L9
- Macquart J.-P., et al., 2010, *Publ. Astron. Soc. Australia*, **27**, 272
- Macquart J. P., et al., 2015, *Advancing Astrophysics with the Square Kilometre Array (AASKA14)*, **p. 55**
- Madau P., Dickinson M., 2014, *ARA&A*, **52**, 415
- Madau P., Pozzetti L., Dickinson M., 1998, *ApJ*, **498**, 106
- Manchester R. N., Fan G., Lyne A. G., Kaspi V. M., Crawford F., 2006, *ApJ*, **649**, 235
- Marshall H. L., Tananbaum H., Avni Y., Zamorani G., 1983, *ApJ*, **269**, 35
- Masui K. W., Sigurdson K., 2015, *Physical Review Letters*, **115**, 121301
- Masui K., et al., 2015, *Nature*, **528**, 523
- McQuinn M., 2014, *ApJ*, **780**, L33
- McQuinn M., Lidz A., Zaldarriaga M., Hernquist L., Hopkins P. F., Dutta S., Faucher-Giguère C.-A., 2009, *ApJ*, **694**, 842
- Metzger B. D., Berger E., Margalit B., 2017, *ApJ*, **841**, 14
- Nakamura O., Fukugita M., Yasuda N., Loveday J., Brinkmann J., Schneider D. P., Shimasaku K., SubbaRao M., 2003, *AJ*, **125**, 1682
- Nakamura O., Fukugita M., Brinkmann J., Schneider D. P., 2004, *AJ*, **127**, 2511
- Nan R., et al., 2011, *International Journal of Modern Physics D*, **20**, 989
- Ng C., et al., 2017, preprint, ([arXiv:1702.04728](https://arxiv.org/abs/1702.04728))
- Niino Y., 2018, *ApJ*, **858**, 4
- Osłowski S., et al., 2018a, *The Astronomer's Telegram*, **11385**
- Osłowski S., et al., 2018b, *The Astronomer's Telegram*, **11396**
- Pen U.-L., Connor L., 2015, *ApJ*, **807**, 179
- Pescalli A., et al., 2016, *A&A*, **587**, A40

- Petroff E., et al., 2015, *MNRAS*, **447**, 246
- Petroff E., et al., 2016, *Publ. Astron. Soc. Australia*, **33**, e045
- Petroff E., et al., 2017, *MNRAS*, **469**, 4465
- Petrosian V., 1976, *ApJ*, **209**, L1
- Planck Collaboration et al., 2016, *A&A*, **594**, A13
- Popov S. B., Postnov K. A., 2010, in Harutyunian H. A., Mickaelian A. M., Terzian Y., eds, *Evolution of Cosmic Objects through their Physical Activity*. pp 129–132 ([arXiv:0710.2006](#))
- Popov S. B., Postnov K. A., 2013, preprint, ([arXiv:1307.4924](#))
- Price D. C., et al., 2018, *The Astronomer’s Telegram*, **11376**
- Ravi V., Shannon R. M., Jameson A., 2015, *ApJ*, **799**, L5
- Ravi V., et al., 2016, *Science*, **354**, 1249
- Rees M. J., 1977, *Nature*, **266**, 333
- Reynolds R. J., 1977, *ApJ*, **216**, 433
- Romero G. E., del Valle M. V., Vieyro F. L., 2016, *Phys. Rev. D*, **93**, 023001
- Rybicki G. B., Lightman A. P., 1986, *Radiative Processes in Astrophysics*. Wiley-VCH
- Schechter P., 1976, *ApJ*, **203**, 297
- Scholz P., et al., 2016, *ApJ*, **833**, 177
- Sembach K. R., et al., 2003, *ApJS*, **146**, 165
- Shand Z., Ouyed A., Koning N., Ouyed R., 2016, *Research in Astronomy and Astrophysics*, **16**, 80
- Shannon R. M., et al., 2017, *The Astronomer’s Telegram*, **11046**
- Shao L., Zhang B., 2017, *Phys. Rev. D*, **95**, 123010
- Shen S., Mo H. J., White S. D. M., Blanton M. R., Kauffmann G., Voges W., Brinkmann J., Csabai I., 2003, *MNRAS*, **343**, 978
- Skilling J., 2004, in Fischer R., Preuss R., Toussaint U. V., eds, *American Institute of Physics Conference Series Vol. 735*, American Institute of Physics Conference Series. pp 395–405, [doi:10.1063/1.1835238](#)
- Spitler L. G., et al., 2014, *ApJ*, **790**, 101
- Spitler L. G., et al., 2016, *Nature*, **531**, 202
- Sun H., Zhang B., Li Z., 2015, *ApJ*, **812**, 33
- Tendulkar S. P., et al., 2017, *ApJ*, **834**, L7
- Thornton D., 2013, PhD thesis, University of Manchester
- Thornton D., et al., 2013, *Science*, **341**, 53
- Tingay S. J., Kaplan D. L., 2016, *ApJ*, **820**, L31
- Totani T., 2013, *PASJ*, **65**, L12
- Verbiest J. P. W., Lorimer D. R., McLaughlin M. A., 2010, *MNRAS*, **405**, 564
- Verbiest J. P. W., Weisberg J. M., Chael A. A., Lee K. J., Lorimer D. R., 2012, *ApJ*, **755**, 39
- Vieyro F. L., Romero G. E., Bosch-Ramon V., Marcote B., del Valle M. V., 2017, *A&A*, **602**, A64
- Wang N., 2017, *Scientia Sinica Physica, Mechanica & Astronomica*, **47**, 059501
- Wang J.-S., Yang Y.-P., Wu X.-F., Dai Z.-G., Wang F.-Y., 2016, *ApJ*, **822**, L7
- Wang W., Luo R., Yue H., Chen X., Lee K., Xu R., 2018, *ApJ*, **852**, 140
- Wei J.-J., Gao H., Wu X.-F., Mészáros P., 2015, *Physical Review Letters*, **115**, 261101
- Willmer C. N. A., 1997, *AJ*, **114**, 898
- Wu X.-F., et al., 2016, *ApJ*, **822**, L15
- Xu J., Han J. L., 2015, *Research in Astronomy and Astrophysics*, **15**, 1629
- Yang Y.-P., Luo R., Li Z., Zhang B., 2017, *ApJ*, **839**, L25
- Yao J. M., Manchester R. N., Wang N., 2017, *ApJ*, **835**, 29
- Young P. J., 1976, *AJ*, **81**, 807
- Yu Y.-W., 2014, *ApJ*, **796**, 93
- Yu Y.-W., Cheng K.-S., Shiu G., Tye H., 2014, *J. Cosmology Astropart. Phys.*, **11**, 40
- Zeilinger W. W., Möller P., Stivielli M., 1993, *MNRAS*, **261**, 175
- Zhang B., 2014, *ApJ*, **780**, L21
- Zhang S.-N., 2016a, preprint, ([arXiv:1601.04558](#))
- Zhang B., 2016b, *ApJ*, **827**, L31
- Zhang B., 2017, *ApJ*, **836**, L32
- Zhang B., 2018a, preprint, ([arXiv:1808.05277](#))
- Zhang B., 2018b, *ApJ*, **854**, L21
- Zheng Z., Ofek E. O., Kulkarni S. R., Neill J. D., Juric M., 2014, *ApJ*, **797**, 71
- Zhou B., Li X., Wang T., Fan Y.-Z., Wei D.-M., 2014, *Phys. Rev. D*, **89**, 107303

APPENDIX A: NOTATIONS USED IN THE CURRENT PAPER

All the notations used in this paper are listed in Table A1.

APPENDIX B: DATA TABLE

The data in the FRB catalogue (Petroff et al. 2016) is given in Table B1. The columns noted as the *Observed parameters* are from the FRB catalogue, while the *Inferred parameters* are computed using the methods in this paper. The inferred parameters are for reference purposes. They are not used in our computation for luminosity functions, as they are *not* needed in the likelihood function Equation (19). The details on how to calculate redshift, luminosity and energy of each FRB are presented in Appendix F.

Table A1. Notations used in the current paper sorted alphabetically.

Notation	Comments
$a(z)$	Scale factor in Cosmology
α	Power-law index of FRB luminosity function
α_e	Power-law index of galaxy electron density profile
BW	Bandwidth of the data, in units of MHz
c	Speed of light in a vacuum in units of cm s^{-1}
$\chi(z)$	Cosmological ionisation fraction as function of redshift z
$\Delta\nu_0 = 1 \text{ GHz}$	Reference spectrum width of FRB
Δt	Time delay in units of ms
DM	Dispersion measure, in units of $\text{cm}^{-3} \text{ pc}$
DM_E	Extragalactic dispersion measure, i.e. $\text{DM}_E = \text{DM} - \text{DM}_{\text{MW}}$
DM_{IGM}	Dispersion measure contribution of IGM
DM_{halo}	Dispersion measure contribution from dark matter halo of the Milky Way
DM_{host}	Dispersion measure contribution of FRB host galaxy
$\text{DM}_{\text{host},0}$	Normalised dispersion measure contribution of FRB host galaxy at redshift of 0 using star formation history
DM_{MW}	Dispersion measure contribution of the Milky way
DM_{src}	Dispersion measure contribution of the local source
EM	Emission measure, in units of $\text{cm}^{-6} \text{ pc}$
\mathcal{E}	Energy, in units of erg
$E(z)$	Logarithmic time derivative of scale factor
ϕ^*	Normalisation factor of luminosity function
ϵ	beam resonance of radio telescope
$f_{\mathcal{D}}$	Distribution function of DM_{host}
f_{IGM}	Baryon mass fraction in the IGM
f_s	Distribution function of DM_{src}
F	Specific fluence, the total energy density of the burst, i.e. the time integrated flux density per unit frequency
$\phi(L)$	Luminosity function
$g(z)$	Electron density per baryon as a function of cosmological redshift z
G	Gain of radio telescope, in units of K Jy^{-1}
h	Dimensionless Hubble parameter, normalised by $100 \text{ km s}^{-1} \text{ Mpc}^{-1}$
H^*	Scale height of disk galaxy
H_0	Hubble constant with $H_0 = 67 \text{ km s}^{-1} \text{ Mpc}^{-1}$
I	Intensity, in units of $\text{erg s}^{-1} \text{ sr}^{-1} \text{ cm}^{-2}$
$I(\text{DM}_E, z)$	Marginalised integral for DM_{src}
$I(\log L)$	Marginalised integral for beam response ϵ
l	integration path length, in units of pc
L	Luminosity, in units of erg s^{-1}
L^*	Upper cut-off luminosity
L_0	Lower cut-off luminosity
Λ	Likelihood function
n_e	Electron density, in units of cm^{-3}
ν	Observing frequency, in units of GHz
n^*	Galaxy density in comoving volume, that is $n^* = \int \phi(L) dL$
N_f	Normalisation factor for likelihood function
M	Absolute stellar magnitude
Ω_b	Dimensionless baryon fraction of Universe. Assumed to be 0.048.
Ω_Λ	Dimensionless cosmological constant. Assumed to be 0.69.
Ω_m	Dimensionless matter fraction of Universe. Assumed to be 0.31.
ϖ	Radius from the z-axis in the cylindrical coordinate.
ϖ^*	Scale radius of the disk galaxy
r	Comoving distance
r_L	Luminosity distance, in terms of comoving distance $r_L = (1+z)r$
R	Radius of galaxy, in units of kpc
R_e	Effective radius of galaxy, in units of kpc
R_{50}	Petrosian radius of galaxy, the radius enclosing 50 percent of petrosian flux
ρ	Stellar density in units of pc^{-3}
SEFD	System equivalent flux density, in units of Jy
SFR(z)	Star formation history as function of redshift in units of $M_\odot \text{ yr}^{-1}$
S_{peak}	Peak flux density of FRB, in units of Jy
T	Temperature of ionised gas
T_{morph}	Morphological index of galaxies
T_{sys}	System temperature of radio receiver, in units of K
Θ	General notation for parameters
θ	Angular distance between FRB and beam centre
θ_b	Beam size of radio telescope
w	FRB duration, in units of ms
\mathcal{W}	General notation for data
z	Cosmological redshift
Z	Vertical distances of FRB to the galaxy disk plane

Table B1. The parameters of known FRBs

FRB	Observed parameters				Inferred parameters						Survey	Reference
	$S_{\text{peak}}^{(a)}$ (Jy)	$w^{(b)}$ (ms)	$F^{(c)}$ (Jy ms)	DM ^(d) (cm^{-3} pc)	DM _E ^(e) (cm^{-3} pc)	DM _E ^(f) (cm^{-3} pc)	$z_{\text{max}}^{(g)}$	$\hat{z}^{(h)}$	$\log \hat{L}_{\text{iso}}^{(i)}$ (erg s^{-1})	$\log \hat{E}_{\text{iso}}^{(j)}$ (erg)		
010125	0.30	9.40 ^{+0.20} _{-0.20}	2.82	790(3)	680	714.09	0.80	0.765 ^{+0.005} _{-0.004}	43.00 ^{+0.29} _{-0.34}	40.75 ^{+0.24} _{-0.33}	Parkes I	[1]
010621	0.41	7.00	2.87	745(10)	222	423.44	0.48	0.443 ^{+0.004} _{-0.082}	42.56 ^{+0.27} _{-0.37}	40.24 ^{+0.27} _{-0.35}	Parkes I	[2][3]
010724	> 30	5.00	>150	375	330.42	280.97	0.33	0.281 ^{+0.003} _{-0.072}	> 43.94	> 41.52	Parkes I	[4]
090625	1.14 ^{+0.42} _{-0.21}	1.92 ^{+0.83} _{-0.77}	2.19 ^{+2.10} _{-1.12}	899.55(1)	867.86	874.07	0.98	0.943 ^{+0.005} _{-0.094}	43.87 ^{+0.28} _{-0.34}	40.84 ^{+0.49} _{-2.84}	Parkes II	[5]
110220	1.30	5.60 ^{+0.10} _{-0.19}	7.28 ^{+0.13} _{-0.13}	944.38(5)	909.61	920.26	1.03	0.995 ^{+0.005} _{-0.004}	43.94 ^{+0.26} _{-0.23}	41.42 ^{+0.18} _{-0.19}	Parkes II	[6]
110523	0.60	1.73 ^{+0.17} _{-0.17}	1.04	623.30(6)	579.78	590.3	0.67	0.628 ^{+0.005} _{-0.089}	43.12 ^{+0.23} _{-0.36}	40.11 ^{+0.26} _{-0.32}	GBT	[7]
110627	0.40	1.40	0.56	723.0(3)	675.54	689.43	0.77	0.738 ^{+0.005} _{-0.091}	43.08 ^{+0.27} _{-0.32}	39.99 ^{+0.27} _{-0.31}	Parkes II	[6]
110703	0.50	4.30	2.15	1103.6(7)	1061.27	1080.52	1.21	1.176 ^{+0.006} _{-0.096}	43.71 ^{+0.27} _{-0.33}	40.97 ^{+0.32} _{-0.29}	Parkes II	[6]
120127	0.50	1.10	0.55	553.3(3)	521.48	532.67	0.60	0.564 ^{+0.005} _{-0.087}	42.90 ^{+0.28} _{-0.36}	39.77 ^{+0.25} _{-0.36}	Parkes II	[6]
121002	0.43 ^{+0.33} _{-0.06}	5.44 ^{+3.50} _{-1.20}	2.34 ^{+4.46} _{-0.77}	1629.18(2)	1554.91	1568.68	1.78	1.749 ^{+0.006} _{-0.098}	44.19 ^{+0.33} _{-0.33}	41.48 ^{+0.62} _{-0.60}	Parkes II	[5][8]
121102	0.40 ^{+0.40} _{-0.10}	3.00 ^{+0.50} _{-0.50}	1.20 ^{+1.60} _{-0.45}	557(2)	369	269.88	0.32	0.268 ^{+0.003} _{-0.070}	42.07 ^{+0.49} _{-0.51}	39.48 ^{+0.56} _{-0.82}	Arecibo	[9]
130626	0.74 ^{+0.49} _{-0.11}	1.98 ^{+1.20} _{-0.44}	1.47 ^{+2.45} _{-0.50}	952.4(1)	885.53	887.31	0.99	0.958 ^{+0.005} _{-0.094}	43.77 ^{+0.47} _{-0.36}	40.77 ^{+0.39} _{-0.64}	Parkes II	[5]
130628	1.91 ^{+0.29} _{-0.23}	0.64 ^{+0.13} _{-0.13}	1.22 ^{+0.47} _{-0.37}	469.88(1)	417.3	422.89	0.48	0.442 ^{+0.004} _{-0.085}	43.28 ^{+0.20} _{-0.34}	39.88 ^{+0.34} _{-0.54}	Parkes II	[5]
130729	0.22 ^{+0.17} _{-0.05}	15.61 ^{+9.98} _{-6.27}	3.43 ^{+6.55} _{-1.81}	861(2)	830	835.58	0.93	0.900 ^{+0.005} _{-0.093}	43.12 ^{+0.40} _{-0.41}	41.05 ^{+0.65} _{-3.05}	Parkes II	[5]
131104	1.12	2.08	2.33	779(1)	707.9	558.8	0.63	0.593 ^{+0.005} _{-0.088}	43.31 ^{+0.26} _{-0.35}	40.46 ^{+0.24} _{-0.36}	Parkes II	[10]
140514	0.47 ^{+0.11} _{-0.08}	2.80 ^{+3.50} _{-0.70}	1.32 ^{+2.34} _{-0.50}	562.7(6)	527.8	538.53	0.61	0.571 ^{+0.005} _{-0.087}	42.95 ^{+0.23} _{-0.38}	40.23 ^{+0.62} _{-0.77}	Parkes II	[11]
150215	0.70 ^{+0.28} _{-0.01}	2.80 ^{+1.20} _{-0.50}	1.96 ^{+1.96} _{-0.37}	1105.6(8)	678.4	812.77	0.91	0.875 ^{+0.005} _{-0.093}	43.66 ^{+0.23} _{-0.29}	40.81 ^{+0.43} _{-0.37}	Parkes II	[14]
150418	2.19 ^{+0.60} _{-0.30}	0.83 ^{+0.25} _{-0.25}	1.82 ^{+1.20} _{-0.72}	776.2(5)	587.7	450.66	0.51	0.473 ^{+0.004} _{-0.084}	43.41 ^{+0.26} _{-0.33}	40.10 ^{+0.46} _{-1.34}	Parkes II	[12]
150610	0.7 ^{+0.30} _{-0.2}	2.0 ^{+1.0} _{-1.0}	> 1.3	1593.9(6)	1486.6	1470.9	1.66	1.631 ^{+0.006} _{-0.097}	44.18 ^{+0.29} _{-0.41}	> 41.04	Parkes II	[18]
150807	128.0 ^{+5.00} _{-5.00}	0.35 ^{+0.05} _{-0.05}	44.80 ^{+8.40} _{-7.90}	266.5(1)	196.5	241.43	0.28	0.235 ^{+0.003} _{-0.067}	44.55 ^{+0.04} _{-0.46}	40.83 ^{+0.33} _{-0.38}	Parkes II	[13]
151206	0.30 ^{+0.04} _{-0.04}	3.0 ^{+0.6} _{-0.6}	> 0.9	1909.8(6)	1666.4	1748.8	2.00	1.971 ^{+0.006} _{-0.097}	44.02 ^{+0.26} _{-0.20}	> 41.07	Parkes II	[18]
151230	0.42 ^{+0.03} _{-0.04}	4.4 ^{+0.5} _{-0.5}	> 1.9	960.4(5)	912.47	922.6	1.03	0.997 ^{+0.005} _{-0.094}	43.38 ^{+0.28} _{-0.15}	> 40.81	Parkes II	[18]
160102	0.5 ^{+0.14} _{-0.5}	3.4 ^{+0.8} _{-0.8}	> 1.8	2596.1(3)	2561.56	2574.3	3.10	3.076 ^{+0.005} _{-0.081}	44.74 ^{+0.27} _{-0.28}	> 41.69	Parkes II	[18]
160317	>3.0	21.00 ^{+7.00} _{-7.00}	>63.0	1165(11)	845.4	770.38	0.86	0.828 ^{+0.005} _{-0.092}	> 44.17	> 42.14	UTMOST	[15]
160410	>7.0	4.00 ^{+1.00} _{-1.00}	>28.0	278(3)	220.3	221.29	0.26	0.211 ^{+0.003} _{-0.064}	> 43.06	> 40.51	UTMOST	[15]
160608	>4.3	9.00 ^{+6.00} _{-6.00}	>38.7	682(7)	443.7	371.69	0.43	0.384 ^{+0.004} _{-0.079}	> 43.44	> 41.24	UTMOST	[15]
170107	22.30	2.60	57.98	609.5(5)	574.5	582.5	0.66	0.620 ^{+0.005} _{-0.088}	44.64 ^{+0.29} _{-0.34}	41.86 ^{+0.28} _{-0.33}	ASKAP	[16]
170827	50.30	0.40	19.87	176.4	139.4	149.4	0.18	0.127 ^{+0.000} _{-0.050}	43.38 ^{+0.33} _{-0.53}	39.89 ^{+0.30} _{-0.46}	UTMOST	[17]
170922	2.30 ^{+0.50} _{-0.50}	26.00	59.80	1111	1066	1078.11	1.20	1.173 ^{+0.006} _{-0.096}	44.35 ^{+0.28} _{-0.33}	42.43 ^{+0.27} _{-0.29}	UTMOST	[19]
171209	0.92	2.5	2.3	1458	1115	1223	1.37	1.339 ^{+0.006} _{-0.097}	44.10 ^{+0.27} _{-0.29}	41.17 ^{+0.25} _{-0.31}	Parkes II	[20]
180301	0.5	3.0	1.5	520	365	287	0.33	0.288 ^{+0.003} _{-0.072}	42.19 ^{+0.30} _{-0.41}	39.55 ^{+0.25} _{-0.37}	Parkes II	[21]
180309	20.8	0.576	11.98	263.47	218.78	233.5	0.27	0.226 ^{+0.003} _{-0.066}	43.56 ^{+0.28} _{-0.42}	40.24 ^{+0.28} _{-0.42}	Parkes II	[22]
180311	0.2	12	2.4	1575.6	1530.3	1543.5	1.75	1.719 ^{+0.006} _{-0.098}	43.70 ^{+0.26} _{-0.28}	41.38 ^{+0.25} _{-0.29}	Parkes II	[23]

(a) peak flux density, (b) burst duration, (c) fluence of burst profile, (d) observed dispersion measure, (e) extragalactic DM computed using the NE2001 model, and (f) extragalactic DM computed using the the YMW16 model, (g) maximum redshift inferred by extragalactic DM using the YMW16 model when assumed $\text{DM}_{\text{host}} = 0$ and $\text{DM}_{\text{src}} = 0$, (h) most probable redshift, (i) most probable isotropic luminosity, (j) most probable isotropic energy.

For calculation of luminosity and energy, we assumed the FRB radiation is isotropic with flat spectrum, and use 1 GHz as the reference value of spectral bandwidth at rest frame of FRBs. The error bar is for 95% confidence level.

The references are, [1] [Burke-Spolaar & Bannister \(2014\)](#), [2] [Keane et al. \(2011\)](#), [3] [Keane et al. \(2012\)](#), [4] [Lorimer et al. \(2007\)](#), [5] [Champion et al. \(2016\)](#), [6] [Thornton et al. \(2013\)](#), [7] [Masui et al. \(2015\)](#), [8] [Thornton \(2013\)](#), [9] [Spitler et al. \(2014\)](#), [10] [Ravi et al. \(2015\)](#), [11] [Petroff et al. \(2015\)](#), [12] [Keane et al. \(2016\)](#), [13] [Ravi et al. \(2016\)](#), [14] [Petroff et al. \(2017\)](#), [15] [Caleb et al. \(2017\)](#), [16] [Bannister et al. \(2017\)](#), [17] [Farah et al. \(2018\)](#), [18] [Bhandari et al. \(2018\)](#), [19] [Farah et al. \(2017\)](#), [20] [Shannon et al. \(2017\)](#), [21] [Price et al. \(2018\)](#), [22] [Osłowski et al. \(2018a\)](#) and [23] [Osłowski et al. \(2018b\)](#).

APPENDIX C: DERIVATION FOR MARGINALISED LIKELIHOOD

Using random variable transformation, we can convert the PDF $f(\log L, r, \text{DM}_{\text{host}}, \text{DM}_{\text{src}}, \log \epsilon)$ to $f(\log S, \text{DM}_{\text{E}}, z, \text{DM}_{\text{src}}, \log \epsilon)$, i.e.

$$f(\log S, \text{DM}_{\text{E}}, z, \text{DM}_{\text{src}}, \log \epsilon) = |\mathbf{J}| f(\log L, r, \text{DM}_{\text{host}}, \text{DM}_{\text{src}}, \log \epsilon), \quad (\text{C1})$$

with the Jacobian determinant

$$|\mathbf{J}| = \begin{vmatrix} \frac{\partial \log L}{\partial \log S} & \frac{\partial \log L}{\partial \text{DM}_{\text{E}}} & \frac{\partial \log L}{\partial z} & \frac{\partial \log L}{\partial \text{DM}_{\text{src}}} & \frac{\partial \log L}{\partial \log \epsilon} \\ \frac{\partial r}{\partial \log S} & \frac{\partial r}{\partial \text{DM}_{\text{E}}} & \frac{\partial r}{\partial z} & \frac{\partial r}{\partial \text{DM}_{\text{src}}} & \frac{\partial r}{\partial \log \epsilon} \\ \frac{\partial \text{DM}_{\text{host}}}{\partial \log S} & \frac{\partial \text{DM}_{\text{host}}}{\partial \text{DM}_{\text{E}}} & \frac{\partial \text{DM}_{\text{host}}}{\partial z} & \frac{\partial \text{DM}_{\text{host}}}{\partial \text{DM}_{\text{src}}} & \frac{\partial \text{DM}_{\text{host}}}{\partial \log \epsilon} \\ \frac{\partial \text{DM}_{\text{src}}}{\partial \log S} & \frac{\partial \text{DM}_{\text{src}}}{\partial \text{DM}_{\text{E}}} & \frac{\partial \text{DM}_{\text{src}}}{\partial z} & \frac{\partial \text{DM}_{\text{src}}}{\partial \text{DM}_{\text{src}}} & \frac{\partial \text{DM}_{\text{src}}}{\partial \log \epsilon} \\ \frac{\partial \log \epsilon}{\partial \log S} & \frac{\partial \log \epsilon}{\partial \text{DM}_{\text{E}}} & \frac{\partial \log \epsilon}{\partial z} & \frac{\partial \log \epsilon}{\partial \text{DM}_{\text{src}}} & \frac{\partial \log \epsilon}{\partial \log \epsilon} \end{vmatrix} \\ = \begin{vmatrix} 1 & 0 & \partial \log L / \partial z & 0 & 1 \\ 0 & 0 & c/H_0 E(z) & 0 & 0 \\ 0 & 1+z & \partial \text{DM}_{\text{host}} / \partial z & -1 & 0 \\ 0 & 0 & 0 & 1 & 0 \\ 0 & 0 & 0 & 0 & 1 \end{vmatrix} \\ = \frac{c(1+z)}{H_0 E(z)}. \quad (\text{C2})$$

Based on the modelling in Section 3, we have

$$f(\log S, \text{DM}_{\text{E}}, z, \text{DM}_{\text{src}}, \log \epsilon) = \phi(\log L) f_r(r) f_{\mathcal{D}}(\text{DM}_{\text{host}}|z) f_s(\text{DM}_{\text{src}}) f_{\epsilon}(\log \epsilon) \frac{c(1+z)}{H_0 E(z)}, \quad (\text{C3})$$

where $\text{DM}_{\text{host}} = (\text{DM}_{\text{E}} - \text{DM}_{\text{IGM}})(1+z) - \text{DM}_{\text{src}}$. The PDF of comoving distance $f_r(r) \propto r^2$ can be re-written as the PDF of redshift, i.e.

$$f_z(z) = f_r(r) \frac{dr}{dz} \propto \frac{c r(z)^2}{H_0 E(z)}. \quad (\text{C4})$$

To get the final likelihood, we need to marginalise the unknown information, i.e. DM_{src} , ϵ , and z . The marginalisation of DM_{src} leads to

$$f(\log S, \text{DM}_{\text{E}}, z, \log \epsilon) = \phi(\log L) f_z(z) I(\text{DM}_{\text{E}}, z) f_{\epsilon}(\log \epsilon) (1+z) \quad (\text{C5})$$

with

$$I(\text{DM}_{\text{E}}, z) = \int_0^{\max(\text{DM}_{\text{src}})} f_{\mathcal{D}}(\text{DM}_{\text{host}}|z) f_s(\text{DM}_{\text{src}}) d\text{DM}_{\text{src}}. \quad (\text{C6})$$

The marginalisation for the beam response (ϵ) gives

$$f(\log S, \text{DM}_{\text{E}}, z) = \int_{-\log 2}^0 f(\log S, \text{DM}_{\text{E}}, z, \log \epsilon) d \log \epsilon \\ = f_z(z) f(\text{DM}_{\text{E}}, z) I(\log L), \quad (\text{C7})$$

with

$$I(\log L) = \int_{-\log 2}^0 \phi(\log L) f_{\epsilon}(\log \epsilon) d \log \epsilon \\ = \frac{1}{\log 2} \left\{ \Gamma \left[\alpha + 1, \frac{L}{L^*} \right] - \Gamma \left[\alpha + 1, \frac{2L}{L^*} \right] \right\}, \quad (\text{C8})$$

where Γ is the incomplete GAMMA function.

Marginalisation of redshift (z) helps to get the final likelihood

$$f(\log S, \text{DM}_{\text{E}}) = \frac{1}{N_f} \int_0^{z_{\text{max}}} f(\log S, \text{DM}_{\text{E}}, z) dz, \quad (\text{C9})$$

where the maximal redshift (z_{max}) in the upper limit of integration is computed by solving $\text{DM}_{\text{E}} - \text{DM}_{\text{IGM}}(z) = 0$. The normalisation factor N_f for the PDF is

$$N_f = \int_{\log S_{\text{min}}}^{\infty} d \log S \int \int \int f(\log S, \text{DM}_{\text{E}}, z, \log \epsilon) d\text{DM}_{\text{E}} dz d \log \epsilon. \quad (\text{C10})$$

After integrating DM_{E} and $\log S$, one gets

$$N_f = \int_0^{z_{\text{max}}} f_z(z) dz \int \Gamma \left[\alpha + 1, \frac{\max(L_0, L_{\text{thre}})}{\epsilon L^*} \right] f_{\epsilon}(\log \epsilon) d \log \epsilon. \quad (\text{C11})$$

where L_0 is the lower cut-off of the luminosity function, $L_{\text{thre}} \equiv 4\pi r_L^2 \Delta\nu_0 S_{\text{min}}$ is the corresponding threshold luminosity for the survey sensitivity at the luminosity distance r_L with a perfect beam response $\epsilon = 1$.

APPENDIX D: AVERAGE ELECTRON DENSITY OF GALAXIES

We estimate the average electron density from the emission measure (EM), i.e. the integration of electron density variance along the line of sight $\text{EM} \equiv \int n_e^2 dr$. EM can be derived from the $\text{H}\alpha$ intensity (Reynolds 1977), i.e.

$$\text{EM} = 2.75 \left(\frac{T}{10^4 \text{ K}} \right)^{0.9} \frac{I_{\text{H}\alpha}}{2.42 \times 10^{-7}} \text{ cm}^{-6} \text{ pc}, \quad (\text{D1})$$

where $I_{\text{H}\alpha}$ is the $\text{H}\alpha$ intensity in units of $\text{erg cm}^{-2} \text{ s}^{-1} \text{ sr}^{-1}$ and T is the ionised gas temperature. $\text{H}\alpha$ intensity ($I_{\text{H}\alpha}$) is calculated from the luminosity via

$$I_{\text{H}\alpha} = \frac{L_{\text{H}\alpha}}{4\pi r^2} = 8 \times 10^{-5} \frac{L_{\text{H}\alpha}}{10^{40} \text{ erg s}^{-1}} \left(\frac{r}{\text{kpc}} \right)^{-2}, \quad (\text{D2})$$

where $r = \eta R$ is the physical size of $\text{H}\alpha$ emission region, in which R and η are the radius of the galaxy and the filling factor respectively. Combining Equation (D2) and Equation (D1), we can derive the average electron density variance

$$\langle n_e^2 \rangle = 1.0 \left(\frac{T}{10^4 \text{ K}} \right)^{0.9} \left(\frac{L_{\text{H}\alpha}}{10^{40} \text{ erg s}^{-1}} \right) \left(\frac{R}{\text{kpc}} \right)^{-3} \text{ cm}^{-6}. \quad (\text{D3})$$

Then the average electron density of the whole galaxy is estimated using $\langle n_e \rangle \simeq \langle n_e^2 \rangle^{1/2} \eta^3$, which leads to Equation (27).

APPENDIX E: DERIVATION OF DM_{IGM}

Here, we calculate DM_{IGM} in a rigorous fashion. To simplify the notations, we use natural units through out this section, where the speed of light $c = 1$.

We assume a Robertson-Walker (RW) metric for the Universe that $ds^2 = -dt^2 + a^2 d\mathbf{x}^2$, where a is the cosmic scale factor, and $d\mathbf{x}$ is the spatial dual basis. The local group velocity of radio wave propagating in the free electron gas is (Rybicki & Lightman 1986)

$$v_g = \left(1 + \frac{\beta n_e}{\nu^2} \right)^{-1}, \quad (\text{E1})$$

where β is the dispersion constant (Lorimer & Kramer 2012) and ν' is the radio wave frequency seen by local observer. The corresponding propagation path associated with the flat-space RW metric is described by the differential equation

$$\frac{dr}{dt} = \frac{1}{a} \nu_g. \quad (\text{E2})$$

As $dz/dt = (1+z)H_0E(z)$ and $1/a = 1+z$, the solution to above differential equation gives

$$r = \int_{z_1}^{z_2} \frac{1}{1 + \beta n_e \nu'^{-2}} \frac{1}{H_0E(z)} dz. \quad (\text{E3})$$

The local electron density is $n_e = \rho_c \Omega_b f_{\text{IGM}} g(z) (1+z)^3 m_p^{-1}$, where f_{IGM} is the cosmological baryon mass fraction in the IGM, the term $(1+z)^3$ comes from the Universe expansion, $\rho_c = 3H_0^2/(8\pi G)$ is the Universe critical density, m_p is the proton mass.

The frequency ν' from an emitter can be derived from the frequency (ν) seen by the Earth observer, i.e. $\nu' = \nu(1+z)$. Thus,

$$r(\nu) = \int_{z_1}^{z_2} \frac{1}{1 + \beta \rho_c \Omega_b m_p^{-1} f_{\text{IGM}} g(z) (1+z) \nu^{-2}} \frac{1}{H_0E(z)} dz. \quad (\text{E4})$$

At infinite frequency,

$$r(\infty) = \int_{z_1}^{z_2} \frac{1}{H_0E(z)} dz. \quad (\text{E5})$$

By comparing Equation (E4) with (E5), the time delay is

$$\Delta t = \frac{\beta}{\nu^2} \int \frac{\rho_c \Omega_b f_{\text{IGM}} g(z) (1+z)}{m_p H_0E(z)} dz, \quad (\text{E6})$$

so that we have

$$\text{DM}_{\text{IGM}} = \int \frac{\rho_c \Omega_b f_{\text{IGM}} g(z) (1+z)}{m_p H_0E(z)} dz, \quad (\text{E7})$$

which gives the same result as Deng & Zhang (2014).

APPENDIX F: THE MOST PROBABLE REDSHIFT, LUMINOSITY AND ENERGY

Using $f_{\mathcal{D}}(\text{DM}_{\text{host}})$, $f_s(\text{DM}_{\text{src}})$ and $f_z(z)$, we can infer the most probable FRB redshift, luminosity, and energy for each FRB individually. Similar methods have been applied to measure the pulsar distance (Verbiest et al. 2010, 2012; Igoshev et al. 2016). We now treat the redshift PDF $f_z(z)$ as the prior. The posterior of redshift given the extragalactic DM becomes

$$f(z|\text{DM}_{\text{E}}) = \frac{1}{N_f} I(\text{DM}_{\text{E}}, z) f_z(z) (1+z) \quad (\text{F1})$$

where $I(\text{DM}_{\text{E}}, z)$ is the given in Equation (C6) and N_f is the corresponding normalisation factor. The most probable redshift maximize the posterior, which leads to

$$\hat{z} = \text{argmax}_z f(z|\text{DM}_{\text{E}}). \quad (\text{F2})$$

One can derive the most probable luminosity with the same method, of which the posterior is

$$f(\log L|\text{DM}_{\text{E}}, \log S) = \frac{1}{N_f} \int f_z(z) (1+z) dz \int f(\text{DM}_{\text{E}}, \log S | \log L, \log \epsilon, z) \cdot f_{\epsilon}(\log \epsilon) d \log \epsilon. \quad (\text{F3})$$

Here we have assumed a uniform prior for $\log L$, and

$$f(\text{DM}_{\text{E}}, \log S | \log L, \log \epsilon, z) \propto \exp \left[-\frac{1}{2} \left(\frac{\Delta S}{\sigma_S} \right)^2 \right] I(\text{DM}_{\text{E}}, z), \quad (\text{F4})$$

with

$$\Delta S = \frac{\epsilon 10^{\log L_{\text{iso}}}}{4\pi r_L^2 \Delta \nu_0} - 10^{\log S}. \quad (\text{F5})$$

The Gaussian likelihood is introduced to include the flux density measurement error (σ_S). For those measurements without the corresponding errorbars, we take 30% as the relative error and compute σ_S .

The intrinsic isotropic energy (\mathcal{E}_{iso}) with a flat spectrum can be computed from the specific influence (F)

$$\mathcal{E}_{\text{iso}} = \frac{F}{1+z} \Delta \nu_0 4\pi r_L^2. \quad (\text{F6})$$

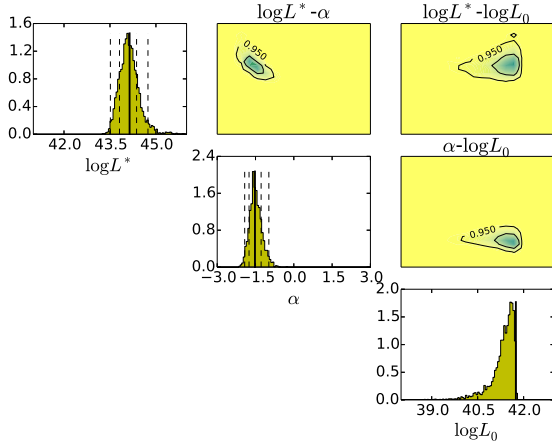
Thus, using a similar likelihood function compared to Equation (F3), replacing L with \mathcal{E} and S with F , the isotropic burst energy can be estimated by F .

All the inferred parameter values are listed in Table B1.

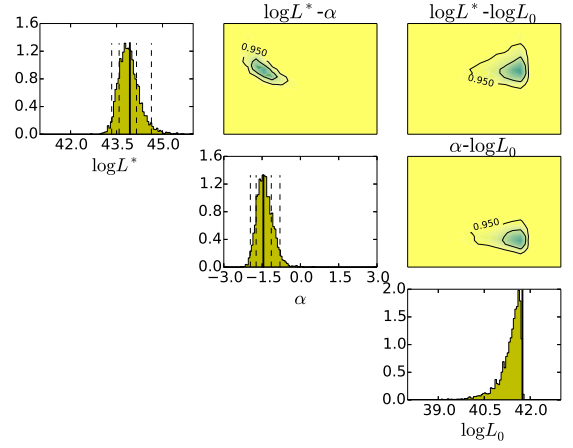
APPENDIX G: POSTERIOR OF FRB LUMINOSITY FUNCTIONS

The posterior distributions of Bayesian analysis are summarised here.

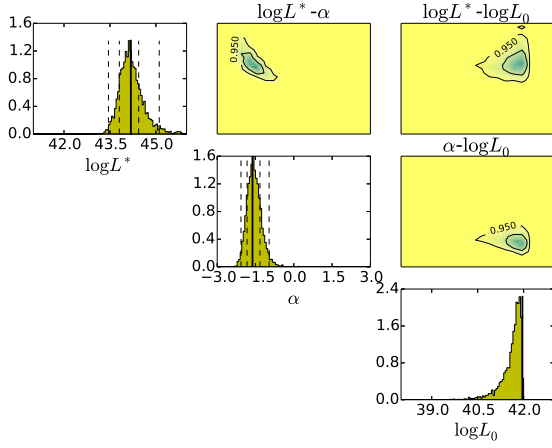
This paper has been typeset from a $\text{\TeX}/\text{\LaTeX}$ file prepared by the author.



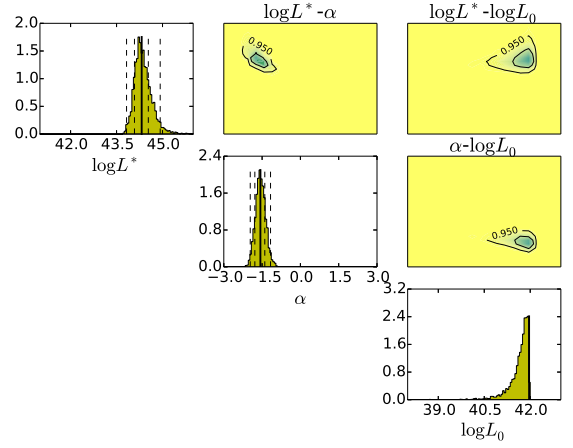
(a) ETGs (NE2001)



(a) LTGs (NE2001)



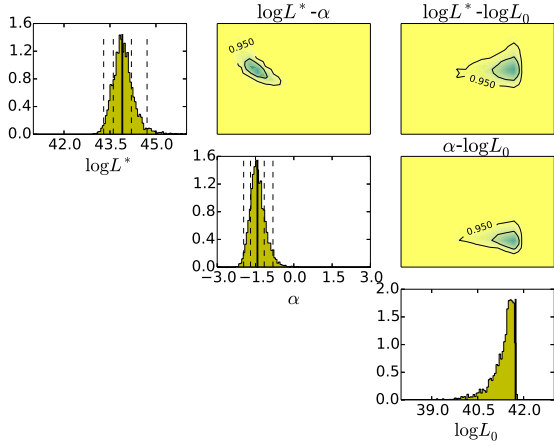
(b) ETGs (YMW16)



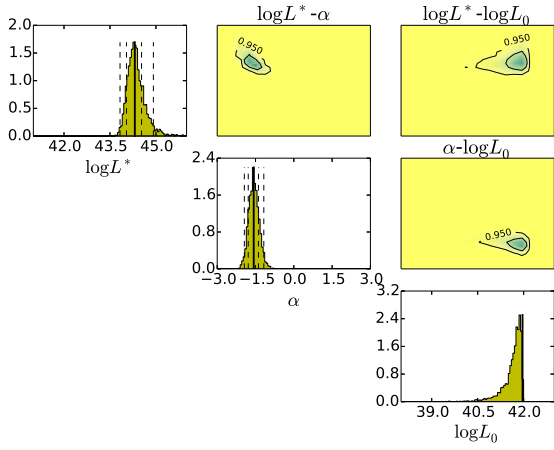
(b) LTGs (YMW16)

Figure G1. The marginalized posterior distribution of ETG luminosity function parameters. The diagonal histogram is the marginalised one-dimensional posterior distribution for each of the parameters. For $\log L^*$ and α , the solid lines denote the most probable parameter value, while the dashed lines indicate the 67% and the 95% confidence level. For $\log L_0$, the solid line denote the upper limit value with 95% confidence level. The off-diagonal contour plots are for the marginalised two-dimensional posteriors, with parameters indicated in the title. The inner and outer black contours are for 67% and 95% confidence levels.

Figure G2. The marginalized posterior distribution of LTG luminosity function parameters. The plots details are the same as Figure G1.



(a) ALGs (NE2001)



(b) ALGs (YMW16)

Figure G3. The marginalized posterior distribution of ALG luminosity function parameters. The plots details are the same as Figure G1.